Human – climate interactions in the central Mediterranean region during the last millennia: The laminated record of Lake Butrint (Albania)

Mario Morellón[1,2*], Flavio S. Anselmetti[3], Daniel Ariztegui[4], Brunhilda Brushulli[5], Gaia Sinopoli[6,7], Bernd Wagner[8], Laura Sadori[6], Adrian Gilli[9], Arben Pambuku[5]

[1] *Instituto de Geociencias (CSIC, UCM),Calle José Antonio Nováis, 2, 3ª planta, 3b. Facultad de Ciencias Geológicas, Univ. Complutense, 28040 Madrid, Spain.*

[2] *Swiss Federal Institute of Aquatic Science and Technology, Eawag, Ueberlandstrasse 133, CH-8600 Dübendorf, Switzerland.*

[3] *Institute of Geological Sciences and Oeschger Centre of Climate Change Research, University of Bern, Baltzerstrasse 1, CH-3012 Bern, Switzerland.*

[4] *Department of Earth Sciences, University of Geneva, Rue des Maraîchers 13, CH-1205 Geneva, Switzerland.*

[5] *Albanian Geological Survey, Rruga e Kavajes, Nr. 153. Tirana, Albania*

[6]*Dipartimento di Biologia Ambientale, Sapienza University of Rome, Italy*

[7]*Dipartimento di Scienze della Terra, Sapienza University of Rome, Italy*

[8] *Department of Geology and Mineralogy, University of Cologne, Cologne, Germany*

[9]*Geological Institute, ETH Zurich, Sonneggstrasse 5, CH-8092 Zurich, Switzerland*

*Corresponding author. E-mail address: mario.morellon@igeo.ucm-csic.es

ABSTRACT

Lake Butrint (39°47 N, 20°1 E) is a ca. 21 m deep, coastal lagoon located in SW Albania where finely-laminated sediments have been continuously deposited during the last millennia. The multi-proxy analysis (sedimentology, high-resolution elemental geochemistry and pollen) of a 12 m long sediment core, supported by seven AMS radiocarbon dates and ^{137}Cs dating, enable a precise reconstruction of the environmental change that occurred in the central Mediterranean region during the last ~4.5 cal kyrs BP. Sediments consist of triplets of authigenic carbonates, organic matter and clayey laminae. Fluctuations in the thickness and/or presence of these different types of seasonal laminae indicate variations in water salinity, organic productivity and runoff in the lake's catchment, as a result of the complex interplay of tectonics, anthropogenic forcing and climate variability. The progradation of the Pavllo river delta, favoured by variable human activity from the nearby ancient city of Butrint, led to the progressive isolation of this hydrological system from the Ionian Sea. The system evolved from an open bay to a restricted lagoon, which is consistent with archaeological data. An abrupt increase in mass-wasting activity between 1515 and 1450 BC, likely caused by nearby seismic activity, led to the accumulation of 24 homogenites, up to 17 cm thick. They have been deposited during the onset of finely laminated sedimentation, which indicates restricted, anoxic bottom water conditions and higher salinity. Periods of maximum water salinity, biological productivity, and carbonate precipitation coincide with warmer intervals, such as the early Roman Warm Period (RWP) (500 BC-0 AD), the Medieval Climate Anomaly (MCA) (800-1400 AD) and recent times (after 1800 AD). Conversely, lower salinity and more oxic conditions, with higher clastic input were recorded during 1400-500 BC, the Late Roman and the Early Medieval periods (0-800 AD) and during the Little Ice Age (1400-1800 AD). Hydrological fluctuations recorded

50 in Butrint are in phase with most central and western Mediterranean records and
51 correlate with NAO variability. In contrast, opposite hydrological patterns have been
52 recorded in the Eastern Balkans and the Levant during the last millennium, emphasizing
53 a complex spatial variability in the region. Phases of maximum settlement intensity in
54 Butrint (Roman-Late Antique) coincide with warmer and/or stable climate periods (0-
55 800 AD and MCA, respectively), indicating a long-term influence of climatic conditions
56 on human activities. The Late Holocene sedimentary record of Lake Butrint
57 demonstrates the complex interplay of climate variability, tectonics and human impact
58 in the recent evolution of coastal Mediterranean regions.

1. INTRODUCTION

During its long history of human occupation, the Mediterranean Basin has experienced significant climate fluctuations with a particularly intense impact in the hydrological cycle (Fletcher and Zielhofer, 2013; Luterbacher et al., 2005). Thus, this region stands out as ideally suited to study the complex interactions between climate variability and human activities during the last millennia (Lavorel et al., 1998; Manning, 2013; McCormick et al., 2012; Roberts et al., 2004), representing the two main factors to drive landscape evolution during the late Holocene (Anthony et al., 2014; Grove and Rackham, 2003).

The Mediterranean coastal areas have been densely populated since prehistoric times, provided essential resources and acted as a natural communication link between the major cultural centres (Marriner et al., 2014). These areas are subjected to an increasing human pressure due to population growth and rising demand for marine resources (UNEP/MAP, 2012) and are threatened by sea level rise in the context of Global Change (Giorgi and Lionello, 2008). Thus, a more detailed knowledge of how climate and ecosystems – including human societies – interacted in the past during phases of environmental change is essential to develop sound adaptation and mitigation policies in these areas.

Sea level rise affected the Mediterranean coastal lowlands by the Holocene marine transgression and led to the formation of inlets, embayments and lagoons (Avramidis et al., 2013). Sediments deposited in these coastal lagoons provide archives of Holocene environmental change, driven by a complex interplay of climate variability, sea level fluctuations, occasional seismic activity (Vött, 2007; Vött et al., 2009) and human impact (Devillers et al., 2015; Koutsodendris et al., 2015). However,

investigated coastal sites in the central and Eastern Mediterranean region are relatively scarce (e.g., Lake Shkodra, Albania (Zanchetta et al., 2012); Amvrakikos Lagoon, Greece (Avramidis et al., 2014); Patria Lagoon, Italy (Sacchi et al., 2014); Larnaca salt lake, Cyprus (Kaniewski et al., 2013) and Syrian coastal plains (Kaniewski et al., 2008) among others (Di Rita and Magri, 2012)) and, if we exclude ancient ports (Marriner and Morhange, 2007; Sadori et al., 2015a), most of the paleoenvironmental information comes from marine cores far offshore and from continental records recovered at highland areas, often subjected to moister and/or colder conditions (Roberts et al., 2008).

Marine records from the Mediterranean region have widely documented the impact of intra-Holocene high-frequency climate variability (Desprat et al., 2013; Rohling et al., 2002). Temperature fluctuations that occurred during the last 2 ka, responding to traditionally identified intervals such as the Medieval Climatic Anomaly (MCA) (950 to 1350 AD) and the Little Ice Age (LIA) (1500 to 1850 AD), with global temperatures above or below average, respectively (Mann and Jones, 2003; Osborn and Briffa, 2006). Continental sequences from the Balkans (e.g., lakes Ohrid (Lacey et al., 2014), Prespa (Leng et al., 2013), Dojran (Zhang et al., 2014)), Anatolia (Fleitmann et al., 2009; Jones et al., 2006; Woodbridge and Roberts, 2011) and the Levant (Bar-Matthews et al., 2003; Migowski et al., 2006a) have recorded a consistent millennial-scale response to a Late Holocene aridification trend within a framework of variable human impact. However, contrasting hydrological patterns have been found locally within this region at shorter timescales during the last millennium (Roberts et al., 2012). Thus, more records from coastal regions are needed to understand Late Holocene environmental changes that occurred in response to climate variability and human impact.

In this study, we investigate a continuous, laminated and high-resolution sedimentary sequence recording environmental change that occurred in the central Mediterranean region during the last ~4.5 cal kyrs BP. We performed a multi-proxy analysis of sediment cores recovered from Lake Butrint (Albania) comprising sedimentologic studies, high-resolution elemental geochemistry, pollen and biogenic silica. Previous studies (Ariztegui et al., 2010) demonstrated the potential of this sequence as an archive of climate variability, human impact and tectonic activity in the region for the last 300 years. The outstanding archaeological sequence of the ancient city of Butrint, located on a peninsula surrounded by the lake waters and continuously occupied since the 6^{th} century BC by Greeks, Romans, Byzantines, Venetians and Ottomans, offers a unique opportunity to discuss the complex interactions between landscape changes and human activities. The paleoenvironmental record of Lake Butrint shows the long-term influence in the sedimentary budget of the lake of geomorphological changes in the catchment that have been modulated by both tectonics and human impact. Along with the short-term impact of climate variability, they are the main drivers of environmental change in Mediterranean coastal areas. The multidisciplinary approach used in this research, together with the finely laminated nature of the sequence, allows a precise identification of the main sediment components associated with different sources and forcing mechanisms, which serve as the agents for environmental reconstructions. Furthermore, the correlation of the reconstructed hydrological fluctuations with other records from the Western and Eastern Mediterranean region suggests a large spatial variability and climatic teleconnections during certain key intervals.

2. REGIONAL SETTING

2.1 Geographical and geological setting

Lake Butrint (39°47 N, 20°1 E) is the southernmost lagoon of the Albanian coast of the Ionian Sea (Fig. 1A), ~5 km north of the Greek Border. It is surrounded by the Vurgu Plain to the north, the Mile Mountains to the east, the Vrina Plain to the south and the Ksamili Peninsula to the west (Tsabaris et al., 2007) (Fig. 1B). The lake basin occupies a N-S extending graben structure formed during the Pleistocene, which has experienced subsidence until recent times and was invaded by Mediterranean Sea water during the Holocene transgression (Aliaj et al., 2001; Meco and Aliaj, 2000). This subsidence led to submerged archaeological Roman and post-Roman remains occurring today below the current water table in the nearby archaeological site of Buthrotum (Lane, 2004).

The bedrock of the lake basin is composed of: i) mid Jurassic to mid Cretaceous limestones, outcropping at the Ksamili Peninsula and the southern part of the Milë Mountain and ii) Paleocene flysch at the northeastern areas of the lagoon (Tsabaris et al., 2007). Butrint is located near the European plate–Adriatic microplate boundary, in one of the most tectonically active regions of the Mediterranean Basin (Meco and Aliaj, 2000; Muço, 1995). Ariztegui et al. (2010) have previously interpreted homogeneous layers within a laminated sequence covering the last ~300 years as earthquake-induced mass-wasting events, coinciding with the historically reported events of 1794, 1811, 1872 and 1917 AD.

2.2. Climate and vegetation

Climate conditions in the region are of Mediterranean type, with a relatively high total annual rainfall ~1500 mm per year, mostly occurring between November and March, and a dry summer season. Mean monthly temperatures range from 9.7 ºC in January to 25.1ºC in August. Southern winds dominate during winter and fall whereas

Northern winds prevail during spring and summer (Lane, 2004). Similarly to other areas of the central and eastern Mediterranean Basin, long-term rainfall variability is mostly related to the North Atlantic Oscillation (NAO) and the Eastern Atlantic pattern (EA) (Lionello et al., 2006).

Vegetation in the surroundings of the lake is highly diverse. Mediterranean maquis occurs mainly in Ksamili Peninsula and in the hills southeast to the lake and is mostly composed of *Quercus coccifera* and minor proportions of *Q. Ilex, Fraxinus ornus, Pistacia lentiscus, Phlomis fruticosa, Colutea arborescens, Phillyrea media*, etc. Small woodland patches occur at the southern and eastern slopes of Sotires Mountain and within the archaeological site, mostly dominated by *Ulmus minor*, *Fraxinus angustifolia*, *Quercus robur*, *Populus alba* and in some cases, *Laurus nobilis* and *Quercus Ilex*. The Vrina Plain area, currently subjected to high salt concentrations and frequent winter flooding, is dominated by halophytic vegetation (*Arthrocnemum* sp., followed by *Juncus* sp. and *Tamarix* sp.). In contrast, typical freshwater marsh vegetation occurs at the northern part of the lake, mainly composed of *Phragmites australis*, *Typha latifolia* and other species, such as *Scirpus lacustris* and *S. maritimus*. Finally, saltmarshes, dominated by glassworts with patches of tamarisk and sea aster, occur as a narrow strip along the south shore of the lagoon, at the mouths of Vivari channel and River Pavllo. Underwater meadows of *Zostera nolti* cover 40-50% of the total surface of the bottom of the lagoon, accompanied by *Ruppia cirrhosa* at deeper areas. The aquatic macrophyte communities in the northern, shallow areas of the lagoon are dominated by *Potamogeton* spp., *Myriophyllum spicatum*, *Nuphar lutea*, and occasionally by associations of *Chara* spp. Algal vegetation changes according to salinity and depth (*Chaetomorpha linum*, *Cladostephus verticillatus*, *Sania rubens*, *Cystoseria* sp. etc.) (ASPBM, 2010; Ramsar, 2003).

182 **2.3. Lake's hydrology and limnology**

183 Butrint is the largest of a series of lagoons along the southernmost part of the
184 Albanian coast and is the only one connected to the Ionian Sea. This connection, the
185 Vivari Channel, is 3.6 km long, 60-100 m wide and up to 6 m deep. The Bistrica River
186 in the North, Milë Mountain in the west and the Pavllo River in the south define the
187 catchment area of the lake (Fig. 1B). Freshwater input into the lake is mainly derived
188 from the Bistrica River and its tributary Kalasa in the northern area, and the Pavllo
189 River and irrigation channels in the Vurgu and Vrina plains (ASPBM, 2010). In
190 addition, the small creeks and springs located at the eastern part of the catchment (Milë
191 Mountains) and Lake Bufi (2.4 m maximum water depth) (Lane, 2004) provide
192 freshwater (Negroni, 2001). Saline waters from the Ionian Sea can occasionally enter
193 into the lake through the Vivari Channel (Fig. 1) during intervals of particularly high
194 tides. The area is currently subjected to microtidal influence with a tidal range of 30 cm
195 (Ariztegui et al., 2010; Hounslow and Chepstow-Lusty, 2004; Negroni, 2001). Thus,
196 freshwater along with occasional marine water input and output, and evaporation
197 output, control variations in the lake's water salinity.

198 The lagoon has a surface of 1600 ha and a water volume of 211×10^6 m^3, with a
199 mean and maximum water depths of 11.4 m and 21.4 m, respectively (Fig. 1C). Strong
200 temperature and salinity gradients led to a meromictic lake with permanent water
201 stratification (Negroni, 2001). The upper ~8 m have seasonal temperature variations
202 between 14 and 25 °C, are oxic (8-9 mg/l) with salinity varying seasonally and laterally
203 between 13 and 26 PSU and pH values ranging from 6.5 to 9.5. Below ~8 m constant
204 temperatures around 17 °C and, anoxic/sulfidic conditions with salinities ranging from
205 30 to 36 PSU prevail (Negroni, 2001). The foot-shaped geometry of the lake, with a N-
206 S orientation of its main axis combined with the freshwater input mostly from the north

and eastern shores result in a rotational movement of surface waters (Negroni, 2001) (Fig. 1B). Vertical mixing of the water column is restricted to the epilimnion. H_2S concentrations in the hypolimnion reach their maximum values near to the lake bottom (>5 mg/l), but in specific cases, deep water can reach the lake's surface and the H_2S is consuming the oxygen in the superficial layer. The lack of oxygen and the presence of H_2S create a situation of asphyxia by causing the dystrophic crises or massive death of fish, mussels and other aquatic organisms. This phenomenon has been recorded several times in the past: 1941, 1955, 1959, 1979, 1980, 1987 and 2008 (ASPBM, 2010; Peja et al., 1996). Lake Butrint has mesotrophic waters becoming almost eutrophic in certain risky areas (Ramsar, 2003).

2.4. Lake evolution and human occupation in the area

The tectonically originated Butrint basin was invaded by Mediterranean waters during the Holocene marine transgression. During the Mid-Holocene, it remained open to the Ionian Sea, forming a large embayment stretching northwards as far as the town of Phoenicê and south towards Mursia (Lane, 2004). However, the progressive aggradation of the Pavllo River delta led to an increasing isolation from the sea (Fig. 1B), as shown by paleogeographical maps based on dated archaeological sites (Martin, 2004). As a result, since Roman times, the Vivari Channel is the only connection to the Ionian Sea. According to archaeological data, only the NE and the SW of the Vrina plain were emerged above sea level during Roman times (Fig. 1B) (Ariztegui et al., 2010; Martin, 2004). A series of boreholes along the margins of the Vrina floodplain clearly indicates the environmental transformation of the area from an open coastal embayment, to estuarine wetlands at ~1270-1390 AD and finally to a river floodplain (Bescoby et al., 2008). Butrint, an important ancient harbor since Greek times declined progressively as it became more isolated from the Ionian Sea.

Although human presence in the Lake Butrint catchment dates from the Paleolithic (Schuldenrein, 2001), first evidences of impact in the landscape were not recorded until the mid to late Bronze Age (after ca. 2000 BC), when slope-derived 'terra rossa' in Konispol Cave (headwaters of Pavllo river) are interpreted as a result of incipient grazing, shepherding and deforestation favored by warmer conditions (Ellwood et al., 1997). The Butrint Peninsula was intermittently occupied during the Bronze Age and the Archaic period (8th century BC) as a hilltop refuge, and a fortified trading post was established by the 6th century BC (Bescoby et al., 2004) (Table 2). By the 4th century BC, Butrint became a Hellenistic port and the city was expanded (Hodges, 2013). A century later (after 31 BC) 'Buthrotum' was designated as a colony for Roman veterans, and the city duplicated its surface towards the Vivary Channel. It also expanded to over 2.5 ha to the Vrina Plain (Bescoby et al., 2004), with the construction of a new aqueduct and bridge across the Vivari Channel (late 1st century AD) (Leppard, 2013; Wilson, 2013). Image analysis of historical aerial photographs revealed a complex farmland divisions in the Vrina Plain during Roman times, responding to a centuriated pattern. The city reached its maximum prosperity as the major port of the Byzantine province of Epirus, until the 550s AD, declining until ~800 AD when a drastic decrease or abandonment of the city and Vrina plain settlements occurred after the attack and sack of the city by the Slavs. This archaeological and documentary hiatus lasted until the late 9th century, when the city was re-occupied by the Byzantines and expanded from the 11th to the 13th centuries and farming activities were intensified again in the Vrina Plain. The city was purchased by Venetians in 1386 AD and declined again until the abandonment of most of the old city in 1572 AD after the Battle of Lepanto, being only lightly settled afterwards (Hodges et al., 2004).

Finally, it was abandoned in the late 18th century, when Ottomans took the power in the region until 1912 AD (Hodges et al., 1996).

3. MATERIALS AND METHODS

A reflection-seismic survey was carried out in June 2011 using a parametric sediment echosounder SES 2000 compact with effective frequencies between 4 and 12 kHz. A total of 30 km of seismic lines were mainly oriented along the two main axis of the lake (N-S and E-W) (Fig. 1D). The data were not compensated for heave and roll and digitally stored. Post-processing was carried out with the INNOMAR software tool ISE 2.5. The sound velocity in the water was assumed to be 1440 m/s and the resulting seismic data set was interpreted using the Kingdom Suite software.

Two overlapping cores (BUT-12-1 AND BUT-12-2) of 12 and 9 m length, respectively, were recovered few meters apart at the deepest area of Lake Butrint using an Uwitec© percussion-coring equipment installed on a floating raft (Fig. 1C). The uppermost part of the sequence was reconstructed using a previously recovered short core BUT-00-2 (Ariztegui et al., 2010). A composite sequence of 11.61 m was obtained, based on the lithostratigraphic correlation of the three cores.

Physical properties (magnetic susceptibility, gamma density, P-wave velocity) were measured on the cores every cm with a Geotek Multi-Sensor Core Logger (MSCL). All cores were subsequently split in two halves and imaged with a Jai CV L105 3 CCD Colour Line Scan Camera with a resolution of 140 ppcm (350 dpi). Colour parameters (L*, a*, b*) were obtained from the core images using LineScan software. Sedimentary facies were defined after visual and microscopic smear slides observations, applying the methodology described in (Schnurrenberger et al., 2003) (Fig. 2).

Elemental composition of the composite sequence was obtained with an AVAATECH XRF core scanner, with a resolution of 1 mm and with two settings: i) with an X-ray current of 1.5 mA, at 30 s count time and 10 kV X-ray voltage for the measurement of Al, Si, P, S, Cl, K, Ca, Ti, V, Cr, Mn, Fe and Rh; and ii) with an X-ray current of 2 mA, at 40 s count time and 30 kV X-ray voltage for the measurement of Zn, Br, Rb, Sr, Zr, Mo, Pb and Bi. The XRF results are expressed in counts per second (cps) and only chemical elements with mean cps over 1500 were considered to be statistically significant.

Cores were sampled every 4 cm for Total Carbon (TC), Total Organic Carbon (TOC), Total Inorganic Carbon (TIC), Total Nitrogen (TN), mineralogical composition, and Biogenic Silica (BiSi); and every 10 cm for pollen, avoiding homogeneous layers for the last three proxies. TC and TN were measured with a HEKAtech Euro EA elemental analyzer. TIC content was determined using a titration coulometer (Coulometric Inc., 5011 CO2-Coulometer) and TOC was calculated as TOC = TC−TIC. Whole sediment mineralogy was characterized by X-ray diffraction with a Bruker-AXS D5005 (working conditions: Cu kα, 40 kV, 30 mA and graphite monochromator) and relative mineral abundance was determined using peak intensity following the procedures described in (Chung, 1974a, b). Results are expressed in percentages with respect to the total dry weight of the sample. BiSi concentrations were measured using a wet chemical digestion technique combined with ICP-AES (Ohlendorf and Sturm, 2008).

For pollen extraction, the sediments were chemically processed using HCl (37%), HF (40%) and hot NaOH (10%). In order to estimate pollen and microcharcoal concentration (number of pollen grains / g), a known amount of *Lycopodium* spores (Stockmarr, 1971) was added to each dry weighted sample. Routine pollen analyses

were carried out using a transmitted light microscope at a magnification of 400X. Pollen identification was based on specialist atlases and on the reference collection of Sapienza University (Rome, Italy). Non Pollen Palynomorphs (NPPs) were counted too. Their percentages have been calculated using a sum including NPPs and pollen of terrestrial plants. 44 pollen analyses have been used to prepare a preliminary pollen diagram. Pollen preservation was partly poor with sometimes very low (< 2000 pollen grains /g) pollen concentration.

The chronology of the lake sequence is based on: i) ^{137}Cs dating in previously recovered core BUT-00-2 and ii) 7 accelerator mass spectrometry (AMS) ^{14}C dates from terrestrial macro-remains and charcoal found in cores BUT-12-1 and 2, analyzed at the ETH Zürich Laboratory of Ion Beam Physics (Table 1). Radiocarbon dates were converted into calendar years BP with the Calib 6.0 software using the INTCAL13 calibration curve (Reimer et al., 2013), selecting the median of the 95.4% distribution (2σ probability interval) (Table 1). The age-depth relationship for the lower part of the sequence was constructed by linear interpolation of calibrated radiocarbon dates using Analyseries (Paillard et al., 1996).

4. RESULTS

4.1 Seismic stratigraphy and sedimentology

The seismic survey indicated low penetration (lower than 5 m) throughout the basin due to gas in the sediments. However, the obtained data allow the identification of relatively steep slopes in the W and E margins of the lake (Fig. 1D), related to the straight margins (N-S oriented) of the lake basin (Fig. 1B). A prominent step on each side (marked with arrows on Fig. 1D) suggests ongoing activity of normal faults responsible for recent tectonic activity and subsidence reported during the last centuries.

These inclined and potentially instable lake slopes might have favored mass-wasting processes leading to the deposition of homogeneous layers intercalated within the laminated sequence (Ariztegui et al., 2010). The alternation of high-amplitude reflections and transparent intervals within the uppermost 2 m of the seismic profiles of the deepest areas of the lake (Fig 1D) results from changing densities likely due to changing lithologies (Fig. 3).

Five sedimentary facies and three sedimentary units were defined and correlated within the sediment cores recovered at the offshore, distal areas of Lake Butrint (Figs. 2 and 3). According to textural and compositional criteria, these facies have been grouped into laminated and massive facies. The first group comprises variegated, finely (facies 1) (Fig 2A-C) to barely laminated (facies 2) (Fig. 2D) silts composed of triplets of: i) light grey clastic-rich laminae, ii) reddish, organic-rich laminae and iii) yellowish, authigenic calcite-rich laminae. The finely laminated facies in the uppermost ~160 cm are proved to represent varves, which were described in detail by Ariztegui et al. (2010). Light grey and reddish laminae are always present within these facies, whereas calcite laminae are absent in some intervals (Fig. 2B-C). The relative thicknesses of each of these laminae are also highly variable throughout the record and can be quantified with colour and compositional analyses (Figs 2 and 3). Massive facies occur as: i) light-grey to brownish, fine-grained and clastic-rich silts (facies 3) (Fig. 2E); ii) variegated, fine-grained and clastic-rich silts organized in fining-upwards successions (facies 4) (Fig. 2F-G) and iii) dark grey to greenish, bioturbated silts with mollusks (facies 5) (Fig. 2H). Facies 3 and 4 are both interpreted as homogenites (i.e. mass-movement-related turbidites; Ariztegui et al., 2010) (Fig. 3) and occur as 1 to 17 cm thick intercalations within the laminated facies (Fig. 2E-G).

352 According to the facies distribution, the sedimentary sequence of Lake Butrint
353 has been divided into 3 main sedimentary units (Figs. 3 and 4):

354 *Unit C (1161.5 – 974.1 cm comp depth), the lowest unit,* is a rather
355 homogeneous interval characterized by facies 5, containing abundant *Scaphopoda* shells
356 and is characterized by the highest proportion of siliciclastic minerals (quartz, feldspars,
357 phyllosilicates), the lowest amount of carbonates (calcite and high-magnesium calcite
358 (HMC)) and pyrite.

359 *Unit B (974.1 – 767.9 cm comp depth)* represents the transitional interval
360 between predominantly massive lower unit C and upper laminated unit A. The lower
361 part of this unit *(subunit B2, 974.1 - 944.6 cm)* is characterized by barely laminated
362 facies 2 with the intercalation of relatively thin (1-5 cm) homogeneous layers (facies 4).
363 The upper part *(subunit B1, 944.6 – 767.9 cm)* is mainly formed by thick grey-clastic
364 and yellow-calcitic laminae (facies 1) with a high number of interspersed, homogeneous
365 layers (facies 5) of variable thickness (2.5 to 17 cm). Unit B displays a gradual but
366 marked upcore increase in calcite content (from 15 to 45%), a higher content on pyrite
367 and scarcer amounts of HMC. Halite, absent in lowermost unit C, is present with low
368 percentages.

369 *Unit A (767.9 – 0 cm comp depth),* the thickest and uppermost interval, is
370 dominated by laminated lithologies. The lower part *(subunit A3, 767.9 – 627.9 cm)*
371 depicts the alternation of barely (2) and finely laminated (1) facies. *Subunit A2 (627.9 –*
372 *361.6 cm)* is composed exclusively by finely laminated facies 1 with few intercalations
373 of homogeneous facies 3, more frequent towards the top. Relatively thicker grey,
374 clastic-rich laminae within facies 1 occur. HMC, halite and pyrite are present in small
375 amounts, with increasing percentages topward. The uppermost *subunit A1 (361.1-0 cm)*

is also composed by finely laminated facies 1 with more frequent intercalations (10) and higher thicknesses (up to 17 cm) of homogeneous facies 3. Thicker and more abundant calcite laminae occur between 340 and 300 cm and through the uppermost 240 cm, coinciding with abrupt increases in calcite (up to 60%). Gypsum, restricted to the uppermost 80 cm, was secondarily precipitated after core BUT00-2 recovery (Fig. 4).

4.2 Physical properties

Bulk magnetic susceptibility is generally low to moderate with values ranging from 0 to 35 10^{-5} SI but shows remarkable variations related to changing lithology through the sequence (Fig. 3). Moderate values (10-40 10^{-5} SI) with little variations occur in basal unit C, as a result of the relatively high clastic content and homogeneous lithology (massive facies 5). Intermediate unit B displays the highest values (up to 170 10^{-5} SI) where abrupt fluctuations and highest values (up to 170 10^{-5} SI) occur, coinciding with the maximum number of homogeneous layers. Uppermost unit A is characterized by much lower and more constant values (0-25 10^{-5} SI). Organic-rich intervals display relative higher values (up to 25 10^{-5} SI), whereas clastic-rich and carbonate-rich intervals are characterized by intermediate (up to 13 10^{-5} SI) and lowest values (<5 10^{-5} SI), respectively (Figs. 3 and 4).

The density curve shows high and more constant values, ranging from 1.20 to 1.60 g/cm^3 in lower units C and B, with higher variations within subunit B1, characterized by alternating facies 1 and 4 (Fig. 3). A decreasing trend occurs along subunits A3 and A2 and high-amplitude variations occur at the uppermost subunit A1. Superimposed on these long-term variations, sharp and abrupt increases (up to 0.20 g/cm^3) occur systematically coinciding with all the homogeneous layers intercalated in units B and A (facies 3 and 4), in contrast with laminated facies (1 and 2). These

contrasting density values in the uppermost part of the sequence might be responsible for the intercalation of high and low amplitude reflections in the seismic profiles of the distal areas of the lake basin (Fig. 1D).

Downcore variations in colour parameters (L*, a*, b*) are closely related with changes in lithology and relative thickness and/or presence of components within laminated facies (Fig. 3). Light grey, clastic-rich intervals are characterized by relatively higher L* values and lowest b* (units C and subunits A3 and most of A2). However, organic-rich intervals are characterized by a higher thickness of brown laminae respect of the other components, as reflected by highest a* peaks, particularly visible when occurring next to lighter-coloured materials (e.g., lower part of subunit A1). In contrast, yellowish carbonate-rich intervals are characterized by maximum b* values, relatively high L* and relatively low a*. Finally, homogeneous layers generally show higher L*, except where these intercalations occur within lighter-coloured facies (e.g., subunit A1).

4.3 Geochemistry

4.3.1 Elemental Geochemistry

XRF core scanner results are shown in Fig. 5. Downcore profiles of elements clearly coincide with the facies distribution: i) Si, Al, K, Ti and to some extent, Fe, show comparatively higher values in clastic-dominated intervals; ii) Ca and Sr display maximum values in carbonate-rich facies; and iii) Fe and Mn show a more complex behavior probably associated with changing redox processes. The first group shows high and rather constant values in basal unit C with also high but much variable values along units B and A. Local abrupt increases associated with homogeneous layers (facies 3 and 4) can be also identified throughout the sequence. Ca displays an opposite trend, reaching maximum values in units B and A1, and secondarily in subunit A2 (Figs. 4 and

5). Sr values show a lower and more constant trend with higher peaks in some of the intervals characterized by high Ca concentrations (uppermost subunits A2 and A1). However, an inverse correlation between Sr and Ca can be observed between 310 and 240 cm most likely due to the replacement of Ca by Sr within calcite crystals. Minor proportions of aragonite, containing Sr, cannot be discarded. In fact, low proportions of this mineral were found in carbonate laminae of the uppermost part of the sequence (Ariztegui et al., 2010). Superimposed on the long-term trends, Fe shows abrupt and maximum increases in subunit B1, where facies 1 and 5 alternate, coinciding with S maxima, likely related to iron sulphide precipitation. In contrast, Mn displays rather low and constant values, relatively higher at lowermost unit C, decreasing upcore, and local, abrupt increases in carbonate and clastic-rich intervals of unit A. Organic-rich intervals are generally depleted in Mn.

Elemental ratios support the previous inferences providing further insights on the geochemical variations recorded in the sequence: higher Ti/Ca ratios in subunits A3 and A2 reflect higher clastic input respect to carbonate-rich A1, whereas most of the maximum peaks correspond to homogeneous layers; highest Si/Ti at the uppermost subunit A1, coinciding with maximum biogenic silica, highlights non-detrital Si and thus evidences an additional (biogenic) source of Si provided by diatoms; and Fe/Mn reaches higher values in organic-rich intervals (subunit A1) and secondarily, in unit B, coinciding with alternating facies 1 and 4 (Figs 4 and 5). Thus Ti/Ca, Si/Ti and Fe/Mn can be interpreted as clastic input, diatom productivity and redox proxies, respectively (Cunningham et al., 2013; Naeher et al., 2013).

4.3.2 Organic geochemistry: C-N-S and BiSi

The TOC content of the Lake Butrint sequence is highly variable, oscillating from 0% to ca 6% (Fig. 4). The organic content of lower units C and B is relatively low and rather constant, increasing in subunit A3 and reaching maximum values at the upper part of subunit A2 and lower subunit A1. TN values, ranging from 0 to 0.4%, mimic the main trends in TOC, with relatively higher content in lower units C and B, evidenced by lower but fluctuating TOC/TN ratios at these intervals. This ratio increases towards the mid part of unit A, slightly decreasing upcore. TOC/TN values range between 6 to 7 at lowermost units A and B, reaching 10 at the mid part of unit A. Typical values for algae are below 10, whereas vascular plants are characterized by ratios higher than 20 (Meyers and Lallier-Vergès, 1999). Thus, the organic matter present in the Lake Butrint sediments is predominantly of lacustrine origin with a minor influence of terrestrial plant remains derived from the catchment, more significant in unit A. A higher, maximum peak of TOC/TN related to a plant-debris-rich layer occurs near to the base of unit A (Fig. 4).

Biogenic silica (BiSi) concentration is rather constant and low in basal unit C, increasing in subunit B1. A return to low values is recorded through subunits A3 and A2. A subsequent abrupt increase occurs in subunit A1, where two relative maxima of 90 and 75 mg/g occur at the intervals 360-340 and 240-180 cm, respectively. After a progressive decreasing trend, BiSi remains constant and centered around 40 mg/g upcore. These discrete BiSi measurements are in good agreement with the Si/Ti ratio determined by XRF core scanning, which underlines the interpretation of this ratio as proxy for the BiSi content. Fluctuations in BiSi reflect changes in diatom primary productivity in the euphotic zone (e.g., (Barker et al., 2013; Johnson et al., 2011)). The similar trends of BiSi and TIC (Fig. 4) suggest that carbonate precipitation in Lake

Butrint is strongly related to diatom productivity by CO_2 uptake, in agreement with the varve-formation model established by Ariztegui et al. (2010).

4.4 Pollen

The pollen record from Butrint is characterized by high fluctuations in concentration (Fig. 6), determined by both continental and marine inputs. Non Pollen Palynomorphs (NPPs) *Glomus* and *Pseudoschizaea* are used to distinguish sources of detrital material. The first is a fungus present in the soil and the second a palynomorph of uncertain origin linked to freshwater input (Medeanic et al., 2008). They are both taken as indicators of erosion. Chenopodiaceae can be used as an indication of water salinity, as many herbs belonging to this family are salt tolerant. *Pinus* (pine) and *Alnus* (alder) deserve other considerations. High percentages of pine pollen cannot be considered representative of the local/regional pollen rain for two reasons: i) the pollen grains found in the Butrint sediments are a mixture of both coastal and montane pines and a high amount was found corroded and fragmented (e.g., wings); and ii) even if regional data from the Balkans suggest that pine forests were widespread in the late Holocene (Kouli, 2012; Panagiotopoulos et al., 2013; Sadori et al., 2015b), the Butrint pine curve does not follow regional trends recorded in other Central Mediterranean sequences. A different explanation is therefore proposed: pine pollen grains are particularly overrepresented in marine sediments because they float on seawater and can therefore be transported long away (e.g., (Combourieu-Nebout et al., 2013; Mercuri et al., 2012). Thus, high percentages of *Pinus* indicate marine water input. Alder grains cannot be ascribed to *Alnus viridis*, a montane alder whose morphology is quite different from that of riparian alders (Giardini et al., 2010). Pollen grains of alder found in Butrint sediments are typical of the riparian trees that can grow along freshwater lakes and rivers. Consequently, increases of alder are either an indication of strong river

input (alder pollen can be transported by rivers into Butrint basin) or more specifically, to the expansion of alder populations related to the development of alluvial plains during phases of delta progradation. In fact, alder and pine never show a similar trend: from the base up to 500 cm depth *Pinus* is prevailing, while alder spreads at the uppermost ~400 cm of the sequence. Single and opposite peaks of the two curves can evidence major continental/marine input. Moreover Alnus is not found in periods of enhanced soil erosion, the last being suggested by increases of Glomus and Pseudoschizaea.

In our pollen diagram a first closure of the bay can be see before 3000 years BP, and is indicated by a sharp increase of pollen grains from inland, namely a reduced contact with marine water. Another important period of water freshening is found around 2200 years BP, and again when the salt water input seems to be quite reduced since the first century AD.

4.5 Chronological model

A total of 37 event layers, deposited instantaneously and represented by massive facies 3 and 4 with a total sediment length of 197.6 cm were subtracted from the sequence for the construction of the age model in order to obtain an event-corrected depth-age scale (Fig. 7A). In the resulting 956.9 cm of sequence (Fig. 7B), the age-depth relationship was constructed by linear interpolation of calibrated radiocarbon dates (Table 1) using Analyseries (Paillard et al., 1996).

The chronology of the lower half of the sequence, represented by units B, C and subunits A2 and A3 is constrained by a total of 5 radiocarbon dates, whereas in the uppermost ca. 5 m of sequence (upper subunit A2 and A1), the chronological control is lower, with 2 radiocarbon dates and the ^{137}Cs maximum activity peaks of 1963 AD and

1986 AD. The constant lithology of the uppermost part of the sequence characterized by finely laminated facies 1 (Fig. 2), together with the good alignment of available dates, points to a rather constant sedimentation rate of ~0.2 cm/year, similar to the rest of unit A and significantly lower than in intermediate unit B (0.38 cm/yr) (Fig. 7B). The good match with annually resolved chronology for the uppermost 300 years (Ariztegui et al., 2010) reinforces the robustness of the age model.

Finally, the age of the base of the sequence was obtained by the extrapolation of the sedimentation rate obtained between the lowermost two radiocarbon dates (0.22 cm/yr). Thus, according to our age model, the 1161.5 cm long sedimentary sequence of Lake Butrint spans the last ~4370 cal years BP (or back to ~2420 BC).

5. DISCUSSION

5.1 The transition from open marine to lagoon conditions (2420-1430 BC)

The oldest recovered sediments (unit C) were deposited under shallow, open-marine conditions as indicated by the massive, bioturbated facies 5, with abundant *Scaphopoda*, typical for sub-tidal conditions of more than 6 m water depth (Brusca and Brusca, 2003; Reynolds, 2002). Relatively low Fe/Mn ratios and relatively poor pollen preservation (Figs. 5 and 8) reflect oxic conditions typical from a shallow, open-marine environment. The abundance of Chenopodiaceae also supports the strong marine influence, whereas high *Pinus* values in the context of low pollen preservation might indicate transport from sea waters. These sedimentological, geochemical, and vegetation patterns coincide with results obtained in the Vrina Plain (Fig. 1B), where mottled, blue-grey clays with abundant mollusks characterize the basal sediments recovered at 3-4 m core depth. These muds, interpreted as marine, are overlain by marsh deposits (Lane, 2004). Additionally, the base of the sedimentary sequence of Lake Bufi

(currently 2 m a.s.l. and located onshore) is characterized by laminated, grey-olive clays with marine ostracod fauna (Lane, 2004). Unfortunately, none of these nearby sequences have an independent, absolute chronology for these marine deposits. In fact, the Lake Bufi age model was obtained by the tuning main vegetation changes with the pollen sequence of Lake Gramousti (Pindus Mountains, NW Greece) (Willis, 1992) assumed to be synchronous. According to this correlation, marine deposits in Lake Bufi were deposited prior to ca. 5000 ^{14}C years BP, equivalent to ~4200-3200 cal years BC, if this date is calibrated with the INTCAL13 curve (Reimer et al., 2013). However, the environmental surveys carried out in the frame of the 1994-1999 archaeological project suggested that a wide lagoon embayment, with marshes in the outlet of Lake Bufi (Fig. 1B), persisted until 1800-1500 BC, as mapped in palaeogeographical reconstructions of the area (Martin, 2004).

This reconstruction is consistent with our age model, according to which first evidences of more restricted and oxygen depleted conditions occurred after ~1620 BC, as indicated by the deposition of barely laminated facies 2, along with the disappearance of marine *Scaphopoda,* an increase in pyrite (Fig. 4) and fluctuating but higher Fe/Mn ratios. A substantial increase in carbonate and halite precipitation indicates significantly higher water salinity (Figs. 4 and 8). Evidences from a first phase of accretion of NW Vrina Plain have been documented through dating of marsh clay underlying the Shën Deli bath-house structure (1500-1800 BC) (Hounslow and Chepstow-Lusty, 2004).

After ~1515 BC, a drastic change in sedimentation occurred: a total of 24 homogeneous layers ranging in thickness from 2.5 to 17 cm were deposited in a very short time (~60 years, according to the age model), coinciding with maximum peaks in magnetic susceptibility (Fig. 3), iron and sulphur (Fig. 5). These homogeneous layers probably result from mass-wasting processes likely triggered by earthquakes shaking

569 the lake basin (Ariztegui et al., 2010), mixing the water column and generating the
570 release of sulphur, extending anoxia to the entire water body and resulting in iron
571 sulphide precipitation. In fact, occasional whole-water column mixing events, releasing
572 H_2S up to the epilimnion and thus causing dystrophic crises, have been reported in
573 Butrint during the 20th century (ASPBM, 2010; Peja et al., 1996). The massive layers
574 are intercalated within finely laminated facies 1, indicative of anoxic conditions, and in
575 this case, with absent organic-rich laminae (Fig. 2F-G), a unique case throughout the
576 record revealing reduced productivity.

577 A strong, documented earthquake (*M = 6.8*), causing coseismic uplift in the less
578 than 6 km distant Corfu Island, was dated at ~1500-1050 BC (Mastronuzzi et al., 2014),
579 as well as a subsequent tsunami responsible for the flooding of Lefkada Island and the
580 Plaghia Peninsula (Greece) (Mastronuzzi et al., 2014; Vött, 2007; Vött et al., 2010; Vött
581 et al., 2009), most probably reaching Southern Albanian coast as well (Fig. 1B).
582 Although this earthquake/tsunami probably affected Lake Butrint, it cannot be identified
583 unambiguously in the sediment core, as there are numerous candidates (homogenous
584 layers) in the respective age window (ca. 60 years) between 945 and 783 cm core depth.
585 A seismic crisis, lasting for a longer period, and leading to the re-activation of
586 subsidence might have decreased the stability of the abrupt slopes of the lake, favouring
587 mass-wasting activity. Nevertheless, the lack of seismic data hampers a full explanation
588 for the origin of these homogenites. Mass wasting activity may have been promoted by
589 increasing subsidence, very active in the basin during the last centuries (Bescoby,
590 2013).

591 **5.2 Climate variability and human impact under lagoon conditions (1430 BC-**
592 **present)**

The deposition of barely laminated facies 2 after 1430 BC indicates more oxic conditions, which is supported by slightly lower Fe/Mn ratios. Increased clastic input and reduced carbonate precipitation, as marked by higher Ti/Ca ratios, also occurred, extending until ~640 BC. These conditions correlate with increasing *Alnus* (and indicators of soil erosion *Glomus* and *Pseudoschizaea*) and decreasing Chenopodiaceae (Figs. 6 and 8). Higher moisture has been also recorded in some areas of the Balkans Region (e.g., Lake Prespa (Leng et al., 2013)), NW Turkey (Fleitmann et al., 2009) or the Levant (Soreq Cave, Israel (Bar-Matthews et al., 2003)), as indicated by relatively lighter $\delta^{18}O$ in all cases. Two wet pulses centered around 850 and 700 BC were also recorded in Kapsia Cave (Peloponnese, Greece) (Finné et al., 2014). A relative increase in humidity, in the context of a longer dry phase, was also recorded in the Albanian Highlands (Lake Maliq, (Fouache et al., 2010)), and in Lake Shkodra (Zanchetta et al., 2012). Evidences of human presence in the region during the mid to late Bronze Age come from Konispol Cave (Schuldenrein, 2001) and from the Butrint Peninsula (Hodges, 2013). However, considering the intermittent character of this occupation and its potential limited impact on the environment, the recorded increase in clastic input cannot be attributed to anthropogenic activities.

5.2.1 Lake Butrint from the Archaic to the Early Medieval period (645 BC – 800 AD)

At ~645 BC, the onset of finely laminated facies 1 reveals more stable and restricted conditions with permanent oxygen-depletion. This change in sedimentation correlates with a slight increase in pyrite content (Fig. 4) and MS (Fig. 3). Subsequently, from ~400 BC to 0 AD, a marked increase in water salinity, indicated by higher Sr and Ca values, and more anoxic conditions, reflected by an increase in TOC and Fe/Mn ratio; occurred. Geochemical evidences correlate with the deposition of

618 thicker, organic-rich laminae within laminated facies 1 and a relative maximum in MS
619 (Fig. 3). Increasing salinity in the lagoon coincides with a general increase in
620 temperature in the Mediterranean region associated with the Roman Warm Period
621 (RWP) (Finné et al., 2011; Manning, 2013). More arid conditions occurred in most of
622 the eastern Mediterranean areas (e.g., Soreq Cave and lakes Van (Wick et al., 2003)
623 and Nar (Dean et al., 2015)) an. In contrast, lighter isotope values have been recorded
624 during this period in Balkan lakes Shkodra (Albania) (Zanchetta et al., 2012), Ohrid
625 (Lacey et al., 2014) and in the Peloponnese (400-100 BC) (Finné et al., 2014). This
626 stage corresponds to the establishment of a Greek harbor (4^{th}-2^{nd} centuries BC) (Hodges
627 et al., 1996) and the foundation and early development of the Roman City of
628 Buthrotum, restricted to the Peninsula (Fig. 1A).

629 A gradual decrease in water salinity, marked by lower Ca and Sr, and more oxic
630 conditions reflected by lower Fe/Mn took place from 0 to ~900 AD. Increasing TOC
631 accompanied by slightly higher TOC/TN reveals an increase in terrestrial organic matter
632 input, which coincides with higher Ti/Ca, indicative of increasing runoff in the Lake
633 Butrint catchment. The observed freshening of the lake waters recorded in Butrint,
634 coincide with interpreted wetter conditions in Balkans lakes Ohrid (Lacey et al., 2014)
635 and Dojran (Zhang et al., 2014) and in Kapsia Cave (NW Greece) (160-300 AD) (Finné
636 et al., 2014).

637 This ca. 1000 yr long period is one of the longest stages characterized by
638 relatively stable environmental conditions throughout the Lake Butrint record (Fig. 8).
639 However, two distinct phases can be identified within this period: i) from 0 to ca. 400
640 AD, characterized by decreasing salinity under moderate clastic input, and ii) from ca.
641 400 to ca. 900 AD, when a marked increase in clastic input, recorded by higher Ti/Ca,
642 likely due to increasing runoff, parallel to decreasing salinity (as indicated by lower Ca

643 and Sr) occurred. The first stage (ca. 0 - 400 AD) covers the second half of the RWP,
644 characterized by generally warm and moist conditions throughout the Mediterranean
645 Basin, with particular stable conditions until the second century AD (Manning, 2013).
646 The second stage (ca 400 – 800 AD), corresponds to the Early Middle Ages (EMA),
647 when a particular increase in moisture occurred in the Eastern Mediterranean region
648 between 350 and 750 AD (Finné et al., 2011). The observed increase in runoff recorded
649 in Butrint, coincide with interpreted wetter conditions in Lake Prespa (Leng et al.,
650 2013); and particularly in Anatolia, such as Lake När (Dean et al., 2015; Jones et al.,
651 2006), Lake Van (Wick et al., 2003), Sofular Cave (Fleitmann et al., 2009) or Bereket
652 Basin (~450-650 AD) (Kaniewski et al., 2007) and the Southern Levant (Soreq Cave
653 (Bar-Matthews et al., 2003) and Dead Sea (Migowski et al., 2006b).

654 In contrast, central and northern Europe experienced colder and arid conditions
655 during the period 400-800 AD, known as the Dark Ages, which might have influenced
656 the migration of northern European tribes into the Western Roman Empire (Büntgen et
657 al., 2011; Cheyette, 2008; McCormick et al., 2012). This dichotomy of 'less favorable'
658 conditions in the Western Mediterranean (Büntgen et al., 2011; Moreno et al., 2012),
659 and a 'more favorable' situation in the East, recorded in the Lake Butrint sequence,
660 might have helped the revival and consolidation of the Eastern Roman Empire (Haldon
661 et al., 2014; Izdebski, 2011; Izdebski et al., 2015; Manning, 2013; McCormick et al.,
662 2012).

663 Additionally, during the 1st century AD, the Roman city expanded to the Vrina
664 Plain (Fig. 1B) and the bridge across the Vivari Channel was constructed (Hodges et al.,
665 1996). The intensification of farming activities in the watershed might be also
666 responsible for the increase in runoff and sediment delivery. In fact, the maximum peak
667 in clastic input, reflected by Ti/Ca ratio, coincides with the maximum occupation of the

city, during late Roman and early Byzantine times (Bescoby et al., 2008; Martin, 2004) (Fig. 8). This stage also correlates with the end of the first synchronous accelerated phase of Pan-Mediterranean delta construction (Maselli and Trincardi, 2013). A short-lived, strong decrease in arboreal pollen was also recorded at the same time (Fig. 6). In contrast, and according to Hounslow and Chepstow-Lusty (2004), the most intense period of siltation recorded in the Vrina Plain, occurred later than recorded in our sequence, from 450 to 1200 AD, with a marked increase in soil input. This discrepancy might be due to a different management of the Pavllo river catchment or to dating uncertainties related with archaeomagnetic dating. Alternatively, a second phase of deforestation related with the revival of Byzantine trade in the region after the late 9th century and/or the intensification of farming during the 11th – 13th centuries AD could explain this increase in erosion (Bescoby, 2013; Hodges et al., 1997; Hounslow and Chepstow-Lusty, 2004). Finally, and according to Bescoby (2013), an earthquake during the 4th century AD (Pavlides and Caputo, 2004) might have caused increased subsidence and substantial damages in public buildings of the city and even the collapse of one of the pillars sustaining the aqueduct, leading to its partial breakdown (Table 2) (Wilson, 2013). However, sedimentological evidences of this seismic event (i.e., homogeneous layers) have not been found in the Lake Butrint record (Figs. 2 and 8).

5.2.2 The Medieval Climate Anomaly (800-1300 AD)

An abrupt increase in Ca and Sr accompanied by a rise in BiSi and a decrease in TOC/TN ratios at ~850 AD (Figs. 3 and 8) indicate higher carbonate precipitation likely related to an increase in diatom productivity. Higher water temperature might have caused this rise in productivity and evaporation, and led to extension of anoxic conditions as marked by higher Fe/Mn and the deposition of more organic-rich, reddish facies 1 (Figs. 5 and 8). Maximum carbonate precipitation occurred between ca. 850 and

1350 AD, with a relative increase in Sr respect to Ca after 1200 AD, indicating highest salinities. This change in water chemistry also coincides with a marked decrease in clastic input, as indicated by lower Ti/Ca, contemporaneous to the decline of the city of Butrint after its sack by the Slavs after ca. 800 AD (Hodges et al., 2009). A strong reduction in pollen concentration has been found after ca. 850 AD (Fig. 6). This decrease might be due to the observed increase in sedimentation rate (Fig. 7) or alternatively, to a reduction of the biomass.

This stage corresponds to the Medieval Climate Anomaly (MCA) (ca. 900-1300 AD), which records a global increase in temperature (Marcott et al., 2013) with different hydrological patterns across the Mediterranean Basin (Moreno et al., 2012; Roberts et al., 2012), Xoplaki et al., in review). Higher sea-surface temperatures have been recorded in the Ionian Sea from the 9^{th} to the 12^{th} centuries AD (Taricco et al., 2009). Grotta Savi speleothem record (SE Alps) has also recorded a marked second warming during the second part of the MCA, from 1150 to 1400 AD (Frisia et al., 2005), coinciding with highest salinities in Butrint. In the Balkans, more positive oxygen isotope compositions of carbonates indicate a more negative water balance in Ohrid (Lacey et al., 2014), and, particularly, in Prespa, where a sharper positive excursion has been recorded (Leng et al., 2013). Consistently, decreased runoff in Lake Dojran (Greece) (Zhang et al., 2014) and more arid conditions occurred in Soreq Cave (Israel) (Bar-Matthews et al., 2003). This pattern, characterized by warmer and more arid conditions matches other continental records from the central (Lake Pergusa, Italy (Sadori et al., this issue)) and W Mediterranean region (Corella et al., 2012; Morellon et al., 2012; Moreno et al., 2012). In contrast, a marked negative isotope excursion, indicating more humid conditions, occurred in Anatolian lakes (Jones et al., 2006; Roberts et al., 2012) contemporaneous to higher humidity in Coastal Syria (Kaniewski

et al., 2011) and higher lake levels in the Dead Sea (Migowski et al., 2006a) during the late phases of the MCA (ca. 1000 – 1450). Predominantly positive North Atlantic Oscillation (NAO) index conditions recorded during this period (Fig. 8) (Olsen et al., 2012; Trouet et al., 2009), might be responsible for the decrease in rainfall at Mediterranean latitudes located in western and central areas, like Butrint and the Balkans.

Several (3) homogeneous layers of up to 10 cm (facies 3) were also deposited in Lake Butrint during the 13th century AD. An increase in seismic activity in the North Ionian Sea and Western Peloponnese area, with earthquakes at 1270 AD, 1278 AD and 1301 AD, has been recorded (Hadler, 2013). The 1278 AD earthquake (M = 6.7) in the nearby Corfu Island was responsible for another tsunami affecting the Ionian Sea coast (Lefkada and Plaghia Peninsula coasts) (Mastronuzzi et al., 2014). These earthquakes might have been responsible for the increase in mass-wasting activity in Butrint. In contrast to previous event(s), sediments display a much lower increase in sulphur. Additionally, the deposition of finely laminated facies resumed afterwards, indicating a shorter and more limited impact, restricted to the mixing of the water-column (Fig. 5). The intense progradation of Bistrica and Pavllo river deltas during the 11th to 13th centuries, likely related to the re-activation of farming in the Vrina Plain might have also contributed to mass-wasting activity, increasing the sensitivity of Butrint to potential triggering mechanisms, such as earthquakes. In fact, sediment cores recovered at the most distal areas of the Vrina Plain, revealed that a swamp was established after 1270-1390 AD (Bescoby et al., 2008). Accordingly, the maximum alluviation of the area, with a location of the delta front similar to the present (Fig 1C), was reached by this time, what is in agreement with results from the Shen-Delli archaeological site (Hounslow and Chepstow-Lusty, 2004). The stabilization of *Alnus* pollen percentages

743 (pollen grains could have a double provenance, both from the inlet rivers and from the
744 riparian belt around the lake) also supports this hypothesis, as it increased gradually
745 since the establishment of lagoon conditions after 1445 BC as a result of the associated
746 increase in habitat for riparian vegetation (Fig. 8).

747 **5.2.3 The Little Ice Age (1300 - 1800 AD)**

748 From the late 14th to 19th centuries AD, carbonate precipitation decreased, as
749 indicated by a gradual decline in Ca and disappearance of Sr, accompanied by more
750 oxic conditions as reflected by a substantial lowering of Fe/Mn (Fig. 8). A slight
751 increase in clastic input, with a relative maximum between 1600 and 1800 AD, reveal a
752 higher hydrological activity in the watershed, which is contemporaneous to this
753 decrease in salinity, indicating more humid conditions. This stage coincides with the
754 Little Ice Age (LIA), a generally cold period (Mann, 2002; Mann et al., 2009), as
755 recorded in the SE Alps (Frisia et al., 2005), the Ionian Sea (Taricco et al., 2009) and
756 the nearby Gulf of Taranto (Grauel et al., 2013), with lower but highly variable
757 temperatures from the 14th to the 19th centuries AD. There are abundant evidences of
758 increased hydrological activity during this period in the western (Morellon et al., 2012;
759 Moreno et al., 2012) and central Mediterranean region (Brown et al., 2013; Giraudi,
760 2014; Wirth et al., 2013), with a marked delta progradation phase in all the southern
761 European deltas (Maselli and Trincardi, 2013).

762 In the Western Balkans, more positive water balances were recorded in Ohrid
763 (Lacey et al., 2014) and Prespa (Leng et al., 2013). In contrast, reduced runoff and more
764 saline waters characterized most sites of the eastern Mediterranean region (e.g., Dojran
765 (Zhang et al., 2014), Lake Nar (Turkey) (Jones et al., 2006), Coastal Syria (Kaniewski
766 et al., 2011), Soreq Cave (Bar-Matthews et al., 2003) and Dead Sea (Migowski et al.,

2006a)). This humid phase correlates with highly variable but generally negative NAO conditions in the region, suggesting an increase in winter rainfall in the region (Trouet et al., 2012) (Fig. 8). Hydrological contrast with neighboring eastern Balkans and Levantine regions likely indicates an eastwards attenuation of the NAO influence in the region (Roberts et al., 2012). In contrast to the previous MCA, the LIA in Butrint is characterized by a more complex internal structure. An initial phase characterized by relatively high Ca levels and a relative maximum in productivity, marked by high BiSi values (Fig. 3) occurs from 1300 to 1600 AD. However, relatively higher clastic input, as reflected by higher Ti/Si and Alnus concentration, accompanied by minima in Ca and BiSi, occurs during the second half of this period, lasting until ~1800 AD. The coldest SST in the Ionian Sea during this period occurred from ca. 1625 to 1875 AD (Taricco et al., 2009), which correlates well with the Lake Butrint record.

Highly variable clastic input during this stage might be also influenced by changing occupation in the area. From the late 16^{th} to 18^{th} centuries, Butrint was actually a Venetian enclave within Ottoman mainland. The area was subjected to periodical Turkish attacks and thus, land use might have experienced fluctuations during this period, until 1797 AD, when Ottomans finally occupied the city (Hodges et al., 1996). Lake Butrint was subsequently subjected to human-made modifications, intensified after the 1930s, including Bistrica River deviation and dredging of sediments from the Vivari Channel (Ariztegui et al., 2010; Peja et al., 1996). Finally, during the 1960s and 1970s the Vrina Plain was drained for the extension of farming during communist times (Hansen et al., 2013). These changes, superimposed to the global temperature increase, enhancing water evaporation, decreased freshwater input and facilitated sea water input, as reflected by recent increases in Ca and Sr. Finally the intensification of farming has contributed to an increase in nutrient load and

792 eutrophication of lake waters, likely corresponding to recent increase in TOC, Fe/Mn
793 and decreasing TOC/TN ratios (Figs. 4 and 8).

794 **5.3 Human - climate interactions in Butrint during historical times**

795 Comparison of fluctuations in estimated settlement intensity in the ancient city
796 of Butrint (Hodges, 2013; Martin, 2004) and associated sites in the Vrina Plain
797 (Bescoby, 2013; Hounslow and Chepstow-Lusty, 2004) (Table 2), based on
798 archaeological and historical records, with environmental changes recorded in the Lake
799 Butrint sediment sequence (Fig. 8), enables investigation in the potential interactions
800 between climatic changes and human activities in the region.

801 In general, warm conditions and periods characterized by higher hydrological
802 stability, marked by relatively low fluctuations in sedimentological and geochemical
803 proxies (Fig. 8); coincide with maximum settlement intensities (Table 2, Fig. 8).
804 Particularly, the interval ca. 0-800 AD is characterized by reduced salinity and increased
805 runoff. During the late Roman Warm Period and the Early Middle Ages, when
806 relatively warm and moist conditions prevailed in the Eastern Mediterranean, Butrint
807 experienced the longest and a quasi-continuous period of maximum occupation, by
808 Roman and Byzantine civilizations. The maximum intensification of farming in the
809 Vrina Plain occurred during the economic revival of the area from ca. 400 to 550 AD
810 (Bescoby, 2013; Hodges, 2013) (Table 2), which is probably reflected by the maximum
811 values in the Ti/Ca ratio, indicative of clastic input (Fig. 8). This increase is not
812 proportional to the decrease in water salinity recorded by Ca and Sr, which reinforces
813 the hypothesis about the anthropogenic contribution to this detrital input. Consistently,
814 the abandonment of the city and associated farms in the catchment after ca. 550 AD,
815 likely as a consequence of the attack of the Ostrogoths in 550 AD (Hodges et al., 1996),

816 is recorded by an abrupt decrease in this proxy, which, however, recovered soon
817 afterwards (Fig. 8). However, a subsequent decrease, coinciding with the decline of the
818 city during the 7th century and extending along the late 9th and 10th centuries, occurred.
819 In fact, references to Butrint disappear during this period from both historical and
820 archaeological sources (Hodges, 2013; Martin, 2004). This archaeological hiatus was
821 not probably caused by a climatic or environmental crisis. It can be almost exclusively
822 attributed to the attack and sack of the city by the Slavs in ca. 800 AD (Hodges et al.,
823 2009).

824 In contrast, the re-occupation of the city of Butrint from the 10th to the 13th
825 century AD, (Hodges and Logue, 2007) (Table 2) occurred in a warm but more unstable
826 period characterized by fluctuating, higher salinity and thus, a more negative water
827 balance (Fig. 8) within the Medieval Climate Anomaly (800-1300 AD). The
828 documented increase in farming practices during the 11th-13th centuries AD in the Vrina
829 Plain is also reflected by an increase in Ti/Ca, contemporaneous to an increase in water
830 salinity in the lake, reflected by highest Sr values recorded during this stage (Fig. 8).
831 This situation demonstrates again that this increase in clastic input had an important
832 anthropogenic contribution, and that, this period of settlement and farming expansion
833 was not significantly favoured by stable or favorable climate conditions. It is also
834 noteworthy that swamps expanded significantly in the distal areas of the Vrina Plain at
835 the end of this phase of farming intensification (Bescoby et al., 2008). This
836 environmental change might be a naturally-driven process due to the continuous
837 progradation of the Pavllo River delta or a consequence of the adoption of different
838 agricultural strategies resulting in an increased sediment loading of inflowing rivers that
839 tipped the environmental balance (Bescoby, 2013). The decline in agricultural

production and food supply to the city cannot be discarded as another factor contributing to the decline of Medieval Butrint.

The subsequent decline of the city of Butrint after the Venetian occupation at ca. 1386 AD coincides with the onset of the Little Ice Age (1300 - 1800 AD), characterized by colder and more humid conditions and lower but highly fluctuating water salinity in the lake (Fig. 8). However, the depopulation and shift of the settlement to the Triangular Fortress (built in the 15th century AD) in the Vivari Channel shore is attributed to the comparatively more important role played by the nearby colony of Corfu (Davies, 2013), rather than to the deterioration of climate experienced in the area. In fact, Butrint was mostly used as a supplier of fish and timber to the island (Crowson, 2007). Thus, the role of this climatic crisis in Butrint decline is highly speculative, considering that it coincides with a period of political instability prior to Venetian occupation (13th century), when the city was located in an area of conflict between Byzantines, Angevines and Venetians. The same applies for the Ottoman occupation at the end of the 18th century, when the ancient city was already abandoned and lower areas were covered by marshes (Bescoby, 2013; Martin, 2004), making the area an inhospitable place.

6. CONCLUSIONS

The sedimentary sequence of Lake Butrint has recorded the progressive isolation of this hydrological system from the Ionian Sea, from an open bay to a restricted lagoon during the last ~4500 cal yrs as a result of the complex interplay of tectonics, climate and human activities.

Shallow-marine, oxic conditions represented by massive-bioturbated silts with *Scaphopoda* occurred until 1620 BC, when the first evidences of isolation from the sea

and oxygen-depleted conditions were recorded. This transitional period terminates around 1515-1450 BC, when multiple mass wasting events lead to the accumulation of 24 massive, homogeneous, up to 17 cm thick homogeneous layers. The M = 6.8 earthquake recorded in Corfu after 1500 BC, responsible for a strong tsunami affecting the Greek Ionian Sea coast, might have been one of the potential trigger mechanisms for these events.

The continuous progradation of the Pavllo River delta to its current location, reached between 1300 and 1600 AD, is reflected by increasing riparian vegetation. The rate of progradation was accelerated after the foundation of the city of Butrint and subsequent farming and urbanization of the Vrina Plain. These changes contributed to an increase in clastic input to the lake with a relative maximum at ca. 550 AD, coinciding with the most intense farming during Late Roman and Early Byzantine occupation.

During the last millennia short-term changes in water chemistry and clastic input in Lake Butrint are mostly controlled by climate fluctuations likely driven by the NAO variability. Periods of maximum water salinity leading to increased carbonate precipitation occurred during the early RWP (500 BC-0 AD), the MCA (800-1400 AD) and during recent times (after 1800 AD), coinciding with warmer periods. The correlation with phases of increased productivity and anoxia reflects diatom activity as the main forcing for carbonate precipitation.

In contrast, fresher conditions with higher clastic input and oxic conditions were recorded during the periods: 1400-500 BC, the Late Roman and Early Middle Ages (0-800 AD) and during the Little Ice Age (1400-1800 AD), reaching coldest and more humid conditions at 1600-1800 AD, in agreement with Ionian Sea SST records.

A good correlation with available sequences from the Western Balkans and the western-central Mediterranean together with the anticorrelated hydrological patterns with Levantine records suggests a spatially variable influence of the NAO in the region during the last millennium.

Periods of maximum settlement intensity (Roman-Late Antique and Medieval) coincide with intervals of climate stability and more positive water balances (~0-800 AD) and warm stages (RWP, EMA and MCA), revealing that favourable climatic conditions facilitated agricultural expansion and economic growth in the Butrint area.

ACKNOWLEDGEMENTS

This paper emerges as a result of a workshop at Costa Navarino and the Navarino Environmental Observatory (NEO), Greece in April 2014, addressing Mediterranean Holocene climate and human societies. The workshop was co-sponsored by PAGES, NEO, the MISTRALS/ PaleoMex program, the Labex OT-Med, the Bolin Centre for Climate Research at Stockholm University, and the Institute of Oceanography at the Hellenic Centre for Marine Research.

Financial support for research was provided by the Spanish Inter-Ministry Commission of Science and Technology (CICYT), through the project HYVARMED (CGL2013-42645-P). M. Morellón holds a 'JAE-DOC' postdoctoral contract co-funded by the Spanish Scientific Research Council (C.S.I.C.) and the European Social Fund. We are grateful to Salvatore Bushati (The Albanian Academy of Sciences) for his support in research activities carried out in Albania and Adrian Dimithri and Marenglen Gjoka (Albanian Geological Survey) for their collaboration in fieldwork in Lake Butrint. We are also grateful to Eawag staff Brian Sinnet for core curation, Irene Brunner for carbon and biogenic silica analyses and Ursula Brupbacher (ETH Zürich,

912 Switzerland) for the assistance with the XRF measurements. Finally, we also
913 acknowledge guest editor, anonymous reviewers and Giovanni Zanchetta (Università di
914 Pisa) for their helpful comments and their criticism, which led to a considerable
915 improvement on this manuscript.

916

917 **REFERENCES**

918

919 Aliaj, S., Baldassare, G., Shkupi, D., 2001. Quaternary subsidence zones in
920 Albania: Some case studies. Bulletin of Engineering Geology and Environment &
921 Behavior 59, 313-318.

922 Anthony, E.J., Marriner, N., Morhange, C., 2014. Human influence and the
923 changing geomorphology of Mediterranean deltas and coasts over the last 6000 years:
924 From progradation to destruction phase? Earth-Science Reviews 139, 336-361.

925 Ariztegui, D., Anselmetti, F.S., Robbiani, J.M., Bernasconi, S.M., Brati, E.,
926 Gilli, A., Lehmann, M.F., 2010. Natural and human-induced environmental change in
927 southern Albania for the last 300 years: constraints from the Lake Butrint sedimentary
928 record. Global and Planetary Change 71, 183-192.

929 ASPBM, 2010. Butrint National Park Management Plan, Albania. Integrated
930 coastal zone management and clean up project. Project ID: PO86807, p. 228.

931 Avramidis, P., Geraga, M., Lazarova, M., Kontopoulos, N., 2013. Holocene
932 record of environmental changes and palaeoclimatic implications in Alykes Lagoon,
933 Zakynthos Island, western Greece, Mediterranean Sea. Quaternary International 293,
934 184-195.

935 Avramidis, P., Iliopoulos, G., Panagiotaras, D., Papoulis, D., Lambropoulou, P.,
936 Kontopoulos, N., Siavalas, G., Christanis, K., 2014. Tracking Mid- to Late Holocene
937 depositional environments by applying sedimentological, palaeontological and

938 geochemical proxies, Amvrakikos coastal lagoon sediments, Western Greece,
939 Mediterranean Sea. Quaternary International 332, 19-36.
940 Bar-Matthews, M., Ayalon, A., Gilmour, M., Matthews, A., Hawkesworth, C.J.,
941 2003. Sea-land oxygen isotopic relationship from planktonic foraminifera and
942 speleothems in the Eastern Mediterranean region and their implication for paleorainfall
943 during interglacial interval. Geochimica et Cosmochimica Acta 67, 3181-3199.
944 Barker, P.A., Hurrell, E.R., Leng, M.J., Plessen, B., Wolff, C., Conley, D.J.,
945 Keppens, E., Milne, I., Cumming, B.F., Laird, K.R., Kendrick, C.P., Wynn, P.M.,
946 Verschuren, D., 2013. Carbon cycling within an East African lake revealed by the
947 carbon isotope composition of diatom silica: a 25-ka record from Lake Challa, Mt.
948 Kilimanjaro. Quaternary Science Reviews 66, 55-63.
949 Bescoby, D., 2013. 2. Landscape and Environmental change: new perspectives,
950 In: Hansen, I.L., Hodges, R., Leppard, S. (Eds.), Butrint 4. The archaeology and
951 histories of an Ionian Town. Oxbox books, Oxford (United Kingdom), pp. 22-30.
952 Bescoby, D., Barclay, J., Andrews, J., 2008. Saints and Sinners: a
953 tephrochronology for Late Antique landscape change in Epirus from the eruptive history
954 of Lipari, Aeolian Islands. Journal of Archaeological Science 35, 2574-2579.
955 Bescoby, D.J., Cawley, G.C., Chroston, P.N., 2004. Enhanced interpretation of
956 magnetic survey data using artificial neural networks: a case study from Butrint,
957 southern Albania. Archaeological Prospection 11, 189-199.
958 Brown, A.G., Hatton, J., Selby, K.A., Leng, M.J., Christie, N., 2013. Multi-
959 proxy study of Holocene environmental change and human activity in the Central
960 Apennine Mountains, Italy. Journal of Quaternary Science 28, 71-82.
961 Brusca, R.C., Brusca, G.J., 2003. Invertebrates, 2 ed. Sinauer Associates,
962 Sunderland, MA (USA).

Büntgen, U., Tegel, W., Nicolussi, K., McCormick, M., Frank, D., Trouet, V., Kaplan, J.O., Herzig, F., Heussner, K.-U., Wanner, H., Luterbacher, J.r., Esper, J., 2011. 2500 Years of European Climate Variability and Human Susceptibility. Science 331, 578-582.

Combourieu-Nebout, N., Peyron, O., Bout-Roumazeilles, V., Goring, S., Dormoy, I., Joannin, S., Sadori, L., Siani, G., Magny, M., 2013. Holocene vegetation and climate changes in the central Mediterranean inferred from a high-resolution marine pollen record (Adriatic Sea). Clim. Past 9, 2023-2042.

Corella, J.P., Brauer, A., Mangili, C., Rull, V., Vegas-Vilarrubia, T., Morellon, M., Valero-Garces, B.L., 2012. The 1.5-ka varved record of Lake Montcortes (southern Pyrenees, NE Spain). Quaternary Research 78, 323-332.

Crowson, A., 2007. Venetian Butrint. Butrint Foundation.

Cunningham, L., Vogel, H., Wennrich, V., Juschus, O., Nowaczyk, N., Rosén, P., 2013. Amplified bioproductivity during Transition IV (332 000–342 000 yr ago): evidence from the geochemical record of Lake El'gygytgyn. Clim. Past 9, 679-686.

Cheyette, F.L., 2008. The disappearance of the ancient landscape and the climatic anomaly of the early Middle Ages: a question to be pursued. Early Medieval Europe 16, 127-165.

Chung, F.H., 1974a. Quantitative interpretation of X-ray diffraction patterns of mixtures. I. Matrix-flushing method for quantitative multicomponent analysis. Journal of Applied Crystallography 7.

Chung, F.H., 1974b. Quantitative interpretation of X-ray diffraction patterns of mixtures. II. Adiabatic principle of X-ray diffraction analysis of mixtures. Journal of Applied Crystallography 7, 526-531.

Davies, S., 2013. 15. Late Venetian Butrint: 16th-18th century, In: Hansen, I.L., Hodges, R., Leppard, S. (Eds.), Butrint 4. The archaeology and histories of an Ionian Town. Oxbow Books, Oxford (United Kingdom), pp. 281-288.

Dean, J.R., Jones, M.D., Leng, M.J., Noble, S.R., Metcalfe, S.E., Sloane, H.J., Sahy, D., Eastwood, W.J., Roberts, C.N., 2015. Eastern Mediterranean hydroclimate over the late glacial and Holocene, reconstructed from the sediments of Nar lake, central Turkey, using stable isotopes and carbonate mineralogy. Quaternary Science Reviews 124, 162-174.

Desprat, S., Combourieu-Nebout, N., Essallami, L., Sicre, M.A., Dormoy, I., Peyron, O., Siani, G., Bout Roumazeilles, V., Turon, J.L., 2013. Deglacial and Holocene vegetation and climatic changes in the southern Central Mediterranean from a direct land–sea correlation. Clim. Past 9, 767-787.

Devillers, B., Brown, M., Morhange, C., 2015. Paleo-environmental evolution of the Larnaca Salt Lakes (Cyprus) and the relationship to second millennium BC settlement. Journal of Archaeological Science: Reports 1, 73-80.

Di Rita, F., Magri, D., 2012. An overview of the Holocene vegetation history from the central Mediterranean coasts. Journal of Mediterranean Earth Sciences 4, 35-52.

Ellwood, B.B., Petruso, K.M., Harrold, F.B., Schuldenrein, J., 1997. High-Resolution Paleoclimatic Trends for the Holocene Identified Using Magnetic Susceptibility Data from Archaeological Excavations in Caves. Journal of Archaeological Science 24, 569-573.

Finné, M., Bar-Matthews, M., Holmgren, K., Sundqvist, H.S., Liakopoulos, I., Zhang, Q., 2014. Speleothem evidence for late Holocene climate variability and floods in Southern Greece. Quaternary Research 81, 213-227.

1013 Finné, M., Holmgren, K., Sundqvist, H.S., Weiberg, E., Lindblom, M., 2011.
1014 Climate in the eastern Mediterranean, and adjacent regions, during the past 6000 years –
1015 A review. Journal of Archaeological Science 38, 3153-3173.
1016 Fleitmann, D., Cheng, H., Badertscher, S., Edwards, R.L., Mudelsee, M.,
1017 Göktürk, O.M., Fankhauser, A., Pickering, R., Raible, C.C., Matter, A., Kramers, J.,
1018 Tüysüz, O., 2009. Timing and climatic impact of Greenland interstadials recorded in
1019 stalagmites from northern Turkey. Geophysical Research Letters 36, n/a-n/a.
1020 Fletcher, W.J., Zielhofer, C., 2013. Fragility of Western Mediterranean
1021 landscapes during Holocene Rapid Climate Changes. Catena 103, 16–29.
1022 Fouache, E., Desruelles, S., Magny, M., Bordon, A., Oberweiler, C., Coussot,
1023 C., Touchais, G., Lera, P., Lézine, A.-M., Fadin, L., Roger, R., 2010.
1024 Palaeogeographical reconstructions of Lake Maliq (Korça Basin, Albania) between
1025 14,000 BP and 2000 BP. Journal of Archaeological Science 37, 525-535.
1026 Giardini, M., Sadori, L., Giraudi, C., Zanchetta, G., 2010. Il paesaggio vegetale
1027 del Gran Sasso d'Italia (Abruzzo, Appennino Centrale) dopo l'eruzione di Agnano
1028 Monte Spina, 105°Congresso Nazionale della Società Botanica Italiana, Milan (Italy), p.
1029 168.
1030 Giorgi, F., Lionello, P., 2008. Climate change projections for the Mediterranean
1031 region. Global and Planetary Change 63, 90-104.
1032 Giraudi, C., 2014. Coarse sediments in Northern Apennine peat bogs and lakes:
1033 New data for the record of Holocene alluvial phases in peninsular Italy. The Holocene
1034 24, 932-943.
1035 Grauel, A.-L., Leider, A., Goudeau, M.-L.S., Müller, I.A., Bernasconi, S.M.,
1036 Hinrichs, K.-U., de Lange, G.J., Zonneveld, K.A.F., Versteegh, G.J.M., 2013. What do
1037 SST proxies really tell us? A high-resolution multiproxy (UK′37, TEXH86 and

foraminifera δ18O) study in the Gulf of Taranto, central Mediterranean Sea. Quaternary Science Reviews 73, 115-131.

Grove, A.T., Rackham, O., 2003. The Nature of Mediterranean Europe: An Ecological History. Yale University Press.

Hadler, H., 2013. Ancient Greek harbours used as geo-archives for palaeotsunami research. Johannes gutenberg-Universität, Mainz (Germany).

Haldon, J., Roberts, N., Izdebski, A., Fleitmann, D., McCormick, M., Cassis, M., Doonan, O., Eastwood, W., Elton, H., Ladstätter, S., Manning, S., Newhard, J., Nicoll, K., Telelis, I., Xoplaki, E., 2014. The Climate and Environment of Byzantine Anatolia: Integrating Science, History, and Archaeology. Journal of Interdisciplinary History 45, 113-161.

Hansen, I.L., Hodges, R., Leppard, S., 2013. Butrint 4: The Archaeology and Histories of an Ionian Town. Oxbow Books for the Butrint Foundation.

Hodges, R., 2013. 1. Excavating away the 'poison': the topographic histoy of Butrint, ancient Buthrotum, In: Hansen, I.L., Hodges, R., Leppard, S. (Eds.), Butrint 4. The archaeology and history of an Ionian town. Oxbow Books, Oxford (United Kingdom), pp. 1-21.

Hodges, R., Bowden, W., Lako, K., 2004. Byzantine Butrint: excavations and surveys 1994-1999. Oxfbow Books, Oxford (United Kingdom).

Hodges, R., Kamani, S., Logue, M., Vroom, J., 2009. The sack of Butrint, c. AD 800. Antiquity 83, project gallery.

Hodges, R., Logue, M., 2007. The Mid-Byzantine re-birth of Butrint. Minerva 18, 41-43.

Hodges, R., Martin, S., Moreland, J., 1996. Butrint (Albania). A microcosm of Mediterranean History. Minerva 7, 9-13.

1063 Hodges, R., Saraci, G., Bowden, W., Chiles, P., Gilkes, O., Lako, K., Lane, A.,
1064 Martin, S., Mitchell, J., Moreland, J., O'Hara, S., Pluciennik, M., Watson, L., 1997.
1065 Late-antique and Byzantine Butrint: interim report on the port and its hinterland (1994–
1066 95). Journal of Roman Archaeology 10, 207-234.
1067 Hounslow, M.W., Chepstow-Lusty, A., 2004. A record of soil loss from Butrint,
1068 southern Albania, using mineral magnetism indicators and charcoal (AD 450 to 1200).
1069 The Holocene 14, 321-333.
1070 Izdebski, A., 2011. Why did agriculture flourish in the late antique East? the role
1071 of climate fluctuations in the development and contraction of agriculture in Asia minor
1072 and the Middle East from the 4th till the 7th c. AD. Millenium. Jahrb. Kult. Gesch.
1073 ersten Jahrtausends Chr 8, 291-312.
1074 Izdebski, A., Pickett, J., Roberts, N., Waliszewski, T., 2015. The environmental,
1075 archaeological and historical evidence for regional climatic changes and their societal
1076 impacts in the Eastern Mediterranean in Late Antiquity. Quaternary Science Reviews in
1077 press.
1078 Johnson, T.C., Brown, E.T., Shi, J., 2011. Biogenic silica deposition in Lake
1079 Malawi, East Africa over the past 150,000 years. Palaeogeography, Palaeoclimatology,
1080 Palaeoecology 303, 103-109.
1081 Jones, M.D., Roberts, C.N., Leng, M.J., Turkes, M., 2006. A high-resolution late
1082 Holocene lake isotope record from Turkey and links to North Atlantic and monsoon
1083 climate. Geology 34, 361-364.
1084 Kaniewski, D., Paulissen, E., De Laet, V., Dossche, K., Waelkens, M., 2007. A
1085 high-resolution Late Holocene landscape ecological history inferred from an
1086 intramontane basin in the Western Taurus Mountains, Turkey. Quaternary Science
1087 Reviews 26, 2201-2218.

1088 Kaniewski, D., Paulissen, E., Van Campo, E., Al-Maqdissi, M., Bretschneider,
1089 J., Van Lerberghe, K., 2008. Middle East coastal ecosystem response to middle-to-late
1090 Holocene abrupt climate changes. Proceedings of the National Academy of Sciences
1091 105, 13941-13946.
1092 Kaniewski, D., Van Campo, E., Guiot, J., Le Burel, S., Otto, T., Baeteman, C.,
1093 2013. Environmental Roots of the Late Bronze Age Crisis. PLoS ONE 8, e71004.
1094 Kaniewski, D., Van Campo, E., Paulissen, E., Weiss, H., Bakker, J., Rossignol,
1095 I., Van Lerberghe, K., 2011. The medieval climate anomaly and the little Ice Age in
1096 coastal Syria inferred from pollen-derived palaeoclimatic patterns. Global and Planetary
1097 Change 78, 178-187.
1098 Kouli, K., 2012. Vegetation development and human activities in Attiki (SE
1099 Greece) during the last 5,000 years. Vegetation History and Archaeobotany 21, 267–
1100 278.
1101 Koutsodendris, A., Brauer, A., Zacharias, I., Putyrskaya, V., Klemt, E.,
1102 Sangiorgi, F., Pross, J., 2015. Ecosystem response to human- and climate-induced
1103 environmental stress on an anoxic coastal lagoon (Etoliko, Greece) since 1930 AD.
1104 Journal of Paleolimnology, 1-16.
1105 Lacey, J., Francke, A., Leng, M., Vane, C., Wagner, B., 2014. A high-resolution
1106 Late Glacial to Holocene record of environmental change in the Mediterranean from
1107 Lake Ohrid (Macedonia/Albania). Int J Earth Sci (Geol Rundsch), 1-16.
1108 Lane, A., 2004. The environs of Butrint 1: The 1995-96 environmental survey,
1109 In: Hodges, R., Bowden, W., Lako, K. (Eds.), Byzantine Butrint: Excavations and
1110 surveys 1994-99. Oxbow Books, Oxford, pp. 27-46.

Lavorel, S., Canadell, J., Rambal, S., Terradas, J., 1998. Mediterranean terrestrial ecosystems: research priorities on global change effects. Global Ecology & Biogeography Letters 7, 157-166.

Leng, M.J., Wagner, B., Boehm, A., Panagiotopoulos, K., Vane, C.H., Snelling, A., Haidon, C., Woodley, E., Vogel, H., Zanchetta, G., Baneschi, I., 2013. Understanding past climatic and hydrological variability in the Mediterranean from Lake Prespa sediment isotope and geochemical record over the Last Glacial cycle. Quaternary Science Reviews 66, 123-136.

Leppard, S., 2013. The Roman Bridge of Butrint, In: Hansen, I.L., Hodges, R., Leppard, S. (Eds.), Butrint 4. The archaeology and histories of an Ionian Town. Oxbow Books, Oxford (United Kingdom), pp. 97-104.

Lionello, P., Malanotte-Rizzoli, P., Boscolo, R., Alpert, P., Artale, V., Li, L., Luterbacher, J., May, W., Trigo, R., Tsimplis, M., Ulbrich, U., Xoplaki, E., 2006. The Mediterranean climate: An overview of the main characteristics and issues, In: P. Lionello, P.M.-R., Boscolo, R. (Eds.), Developments in Earth and Environmental Sciences. Elsevier, pp. 1-26.

Luterbacher, J., Xoplaki, E., Casty, C., Wanner, H., Pauling, A., Küttel, M., Rutishauser, T., Brönnimann, S., Fischer, E., Fleitmann, D., González-Rouco, F.J., García-Herrera, R., Barriendos, M., Rodrigo, F., Gonzalez-Hidalgo, J.C., Saz, M.A., Gimeno, L., Ribera, P., Brunet, M., Paeth, H., Rimbu, N., Felis, T., Jacobeit, J., Dünkeloh, A., Zorita, E., Guiot, J., Türkes, M., Alcoforado, M.J., Trigo, R., Wheeler, D., Tett, S., Mann, M.E., Touchan, R., Shindell, D.T., Silenzi, S., Montagna, P., Camuffo, D., Mariotti, A., Nanni, T., Brunetti, M., Maugeri, M., De Zerefos, C., Zolt, S., Lionello, P., 2005. Mediterranean Climate Variability Over The Last Centuries: A Review, In: Lionello, P., Malanotte-Rizzoli, P., Boscolo, R. (Eds.), The Mediterranean

1136 Climate: an overview of the main characteristics and issues. Elsevier, Amsterdam (The
1137 Netherlands), pp. 27-148.
1138 Mann, M.E., 2002. Little Ice Age, In: MacCracken, M.C., Perry, J.S. (Eds.),
1139 Encyclopedia of Global Environmental Change, pp. 504–509.
1140 Mann, M.E., Jones, P.D., 2003. Global surface temperatures over the past two
1141 millennia. Geophys. Res. Lett. 30, 1820.
1142 Mann, M.E., Zhang, Z., Rutherford, S., Bradley, R.S., Hughes, M.K., Shindell,
1143 D., Ammann, C., Faluvegi, G., Ni, F., 2009. Global Signatures and Dynamical Origins
1144 of the Little Ice Age and Medieval Climate Anomaly. Science 326, 1256-1260.
1145 Manning, S., 2013. The Roman World and Climate: Context, Relevance of
1146 Climate Change, and Some Issues, In: Harris, W. (Ed.), The Ancient Mediterranean
1147 Environment between Science and History. Brill, Leiden, The Netherlands, pp. 103-
1148 170.
1149 Marcott, S.A., Shakun, J.D., Clark, P.U., Mix, A.C., 2013. A Reconstruction of
1150 Regional and Global Temperature for the Past 11,300 Years. Science 339, 1198-1201.
1151 Marriner, N., Morhange, C., 2007. Geoscience of ancient Mediterranean
1152 harbours. Earth-Science Reviews 80, 137-194.
1153 Marriner, N., Morhange, C., Kaniewski, D., Carayon, N., 2014. Ancient harbour
1154 infrastructure in the Levant: tracking the birth and rise of new forms of anthropogenic
1155 pressure. Sci. Rep. 4.
1156 Martin, S., 2004. The topography of Butrint, In: Hodges, R., Bowden, W., Lako,
1157 K. (Eds.), Byzantine Butrint: Excavations and surveys 1994-99. Oxbow Books, Oxford
1158 (United Kingdom), pp. 76-103.
1159 Maselli, V., Trincardi, F., 2013. Man made deltas. Sci. Rep. 3.

1160 Mastronuzzi, G., Calcagnile, L., Pignatelli, C., Quarta, G., Stamatopoulos, L.,
1161 Venisti, N., 2014. Late Holocene tsunamogenic coseismic uplift in Kerkira Island,
1162 Greece. Quaternary International 332, 48-60.
1163 McCormick, M., Büntgen, U., Cane, M.A., Cook, E.R., Harper, K., Huybers, P.,
1164 Litt, T., Manning, S.W., Mayewski, P.A., More, A.F.M., Nicolussi, K., Tegel, W., 2012.
1165 Climate Change during and after the Roman Empire: Reconstructing the Past from
1166 Scientific and Historical Evidence. Journal of Interdisciplinary History 43, 169-220.
1167 Meco, S., Aliaj, S., 2000. Geology of Albania, Stuttgart.
1168 Mercuri, A.M., Bandini Mazzanti M., Torri, P., Vigliotti, L., Bosi, G.,
1169 Florenzano, A., Olmi L., Massamba N'siala, I., 2012. A marine/terrestrial integration
1170 for mid-late Holocene vegetation history and the development of the cultural landscape
1171 in the Po valley as a result of human impact and climate change. Vegetation History and
1172 Archaeobotany 21, 353-372.
1173 Meyers, P.A., Lallier-Vergès, E., 1999. Lacustrine sedimentary organic matter
1174 records of Late Quaternary paleoclimates. Journal of Paleolimnology 21, 345-372.
1175 Migowski, C., Stein, M., Prasad, S., Negendank, J.F.W., Agnon, A., 2006a.
1176 Holocene climate variability and cultural evolution in the Near East from the Dead Sea
1177 sedimentary record. Quaternary Research 66, 421-431.
1178 Migowski, C., Stein, M., Prasad, S., Negendank, J.F.W., Agnon, A., 2006b.
1179 Holocene climate variability and cultural evolution in the Near East from the Dead Sea
1180 sedimentary record. Quaternary Research
1181 Holocene Climate and Cultural Evolution in Late Prehistoric-Early Historic
1182 West Asia 66, 421-431.
1183 Morellon, M., Perez-Sanz, A., Corella, J.P., Buentgen, U., Catalan, J., Gonzalez-
1184 Samperiz, P., Gonzalez-Trueba, J.J., Lopez-Saez, J.A., Moreno, A., Pla-Rabes, S., Saz-

1185 Sanchez, M.A., Scussolini, P., Serrano, E., Steinhilber, F., Stefanova, V., Vegas-
1186 Vilarrubia, T., Valero-Garces, B., 2012. A multi-proxy perspective on millennium-long
1187 climate variability in the Southern Pyrenees. Climate of the Past 8, 683-700.
1188 Moreno, A., Pérez, A., Frigola, J., Nieto-Moreno, V., Rodrigo-Gámiz, M.,
1189 Martrat, B., González-Sampériz, P., Morellón, M., Martín-Puertas, C., Corella, J.P.,
1190 Belmonte, Á., Sancho, C., Cacho, I., Herrera, G., Canals, M., Grimalt, J.O., Jiménez-
1191 Espejo, F., Martínez-Ruiz, F., Vegas-Vilarrúbia, T., Valero-Garcés, B.L., 2012. The
1192 Medieval Climate Anomaly in the Iberian Peninsula reconstructed from marine and lake
1193 records. Quaternary Science Reviews 43, 16-32.
1194 Muço, B., 1995. The seasonality of Albanian earthquakes and cross-correlation
1195 with rainfall. Physics of the Earth and Planetary Interiors 88, 285-291.
1196 Naeher, S., Gilli, A., North, R.P., Hamann, Y., Schubert, C.J., 2013. Tracing
1197 bottom water oxygenation with sedimentary Mn/Fe ratios in Lake Zurich, Switzerland.
1198 Chemical Geology 352, 125-133.
1199 Negroni, G., 2001. La Laguna di Butrinti. Il Pesce 6, 45-49.
1200 Ohlendorf, C., Sturm, M., 2008. A modified method for biogenic silica
1201 determination. Journal of Paleolimnology 39, 137-142.
1202 Olsen, J., Anderson, N.J., Knudsen, M.F., 2012. Variability of the North Atlantic
1203 Oscillation over the past 5,200 years. Nature Geosci 5, 808-812.
1204 Osborn, T.J., Briffa, K.R., 2006. The Spatial Extent of 20th-Century Warmth in
1205 the Context of the Past 1200 Years. Science 311, 841-844.
1206 Paillard, D., Labeyrie, L., Yiou, P., 1996. Analyseries 1.0: a Macintosh software
1207 for the analysis of geographical time-series. Eos 77, 379.

1208 Panagiotopoulos, K., Aufgebauer, A., Schäbitz, F., Wagner, B., 2013.
1209 Vegetation and climate history of the Lake Prespa region since the Lateglacial.
1210 Quaternary International 293, 157-169.
1211 Pavlides, S., Caputo, R., 2004. Magnitude versus faults' surface parameters:
1212 quantitative relationships from the Aegean Region. Tectonophysics 380, 159-188.
1213 Peja, N., Vaso, A., Miho, A., Rakaj, N., Crivelli, A.J., 1996. Characteristics of
1214 Albanian lagoons and their fisheries. Fisheries Research 27, 215-225.
1215 Powell, A., 2004. The faunal remains, In: Hodges, R., Bowden, W., Lako, K.
1216 (Eds.), Byzantine Butrint. Excavation and Surveys. Oxbow Books, Oxford (United
1217 Kingdom), pp. 305-320.
1218 Ramsar, 2003. Information sheet on Ramsar wetlands: Butrint (Albania), p. 15.
1219 Reimer, P.J., Bard, E., Bayliss, A., Beck, J.W., Blackwell, P.G., Bronk Ramsey,
1220 C., Buck, C.E., Cheng, H., Edwards, R.L., Friedrich, M., Grootes, P.M., Guilderson,
1221 T.P., Haflidason, H., Hajdas, I., Hatté, C., Heaton, T.J., Hoffmann, D.L., Hogg, A.G.,
1222 Hughen, K.A., Kaiser, K.F., Kromer, B., Manning, S.W., Niu, M., Reimer, R.W.,
1223 Richards, D.A., Scott, E.M., Southon, J.R., Staff, R.A., Turney, C.S.M., van der Plicht,
1224 J., 2013. IntCal13 and Marine13 Radiocarbon Age Calibration Curves 0–50,000 Years
1225 cal BP.
1226 Reynolds, P.D., 2002. The scaphopoda, In: A.J. Southward,
1227 P.A.T.C.M.Y.L.A.F. (Ed.), Advances in Marine Biology. Academic Press, pp. 137-236.
1228 Roberts, N., Jones, M.D., Benkaddour, A., Eastwood, W.J., Filippi, M.L.,
1229 Frogley, M.R., Lamb, H.F., Leng, M.J., Reed, J.M., Stein, M., Stevens, L., Valero-
1230 Garcés, B., Zanchetta, G., 2008. Stable isotope records of Late Quaternary climate and
1231 hydrology from Mediterranean lakes: the ISOMED synthesis. Quaternary Science
1232 Reviews 27, 2426-2441.

1233 Roberts, N., Moreno, A., Valero-Garcés, B.L., Corella, J.P., Jones, M., Allcock,
1234 S., Woodbridge, J., Morellón, M., Luterbacher, J., Xoplaki, E., Türkeş, M., 2012.
1235 Palaeolimnological evidence for an east–west climate see-saw in the Mediterranean
1236 since AD 900. Global and Planetary Change 84-85, 23-24.
1237 Roberts, N., Stevenson, T., Davis, B., Cheddadi, R., Brewster, S., Rosen, A.,
1238 2004. Holocene climate, environment, and cultural change in the circum-Mediterranean
1239 region, In: Battarbee, R.W., Gasse, F., Stickley, C.E. (Eds.), Past climate variability
1240 through Europe and Africa. Springer, Dordrecht, The Netherlands, pp. 343-362.
1241 Rohling, E., Mayewski, P., Abu-Zied, R., Casford, J., Hayes, A., 2002.
1242 Holocene atmosphere-ocean interactions: records from Greenland and the Aegean Sea.
1243 Climate Dynamics 18, 587-593.
1244 Sacchi, M., Molisso, F., Pacifico, A., Vigliotti, M., Sabbarese, C., Ruberti, D.,
1245 2014. Late-Holocene to recent evolution of Lake Patria, South Italy: An example of a
1246 coastal lagoon within a Mediterranean delta system. Global and Planetary Change 117,
1247 9-27.
1248 Sadori, L., Allevato, E., Bellini, C., Bertacchi, A., Boetto, G., Di Pasquale, G.,
1249 Giachi, G., Giardini, M., Masi, A., Pepe, C., Russo Ermolli, E., Mariotti Lippi, M.,
1250 2015a. Archaeobotany in Italian ancient Roman harbours. Review of Palaeobotany and
1251 Palynology in press.
1252 Sadori, L., Giardini, M., Gliozzi, E., Mazzini, I., Sulpizio R., van Welden, A.,
1253 Zanchetta, G., 2015b. Vegetation, climate and environmental history of the last 4500
1254 years at lake Shkodra (Albania/Montenegro). The Holocene 25, 435-444.
1255 Sadori, L., Giraudi, C., Masi, A., Magny, M., Ortu, E., Zanchetta, G., Izdebski,
1256 A., this issue. Climate, environment and society in Southern Italy during the last 2000

years. A review of the environmental, historical and archaeological evidence. Quaternary Science Reviews.

Schnurrenberger, D., Russell, J., Kelts, K., 2003. Classification of lacustrine sediments based on sedimentary components. Journal of Paleolimnology 29, 141-154.

Schuldenrein, J., 2001. Stratigraphy, sedimentology, and site formation at Konispol Cave, Southwest Albania. Geoarchaeology 16, 559-602.

Stockmarr, J., 1971. Tables with spores used in absolute pollen analysis. Pollen and Spores 13, 614-621.

Taricco, C., Ghil, M., Alessio, S., Vivaldo, G., 2009. Two millennia of climate variability in the Central Mediterranean. Clim. Past 5, 171-181.

Trouet, V., Esper, J., Graham, N.E., Baker, A., Scourse, J.D., Frank, D.C., 2009. Persistent Positive North Atlantic Oscillation Mode Dominated the Medieval Climate Anomaly. Science 324, 78-80.

Trouet, V., Scourse, J.D., Raible, C.C., 2012. North Atlantic storminess and Atlantic Meridional Overturning Circulation during the last Millennium: Reconciling contradictory proxy records of NAO variability. Global and Planetary Change 84–85, 48-55.

Tsabaris, C., Eleftheriou, G., Kapsimalis, V., Anagnostou, C., Vlastou, R., Durmishi, C., Kedhi, M., Kalfas, C.A., 2007. Radioactivity levels of recent sediments in the Butrint Lagoon and the adjacent coast of Albania. Applied Radiation and Isotopes 65, 445-453.

UNEP/MAP, 2012. State of the Mediterranean Marine and Coastal Environment,, Athens (Greece), p. 96.

Vött, A., 2007. Relative sea level changes and regional tectonic evolution of seven coastal areas in NW Greece since the mid-Holocene. Quaternary Science Reviews 26, 894-919.

Vött, A., Bareth, G., Brückner, H., Curdt, C., Fountoulis, I., Grapmayer, R., Hadler, H., Hoffmeister, D., Klasen, N., Lang, F., Masberg, P., May, S.M., Ntageretzis, K., Sakellariou, D., Willershäuser, T., 2010. Beachrock-type calcarenitic tsunamites along the shores of the eastern Ionian Sea (western Greece) – case studies from Akarnania, the Ionian Islands and the western Peloponnese. Zeitschrift f??r Geomorphologie, Supplementary Issues 54, 1-50.

Vött, A., Brückner, H., Brockmüller, S., Handl, M., May, S.M., Gaki-Papanastassiou, K., Herd, R., Lang, F., Maroukian, H., Nelle, O., Papanastassiou, D., 2009. Traces of Holocene tsunamis across the Sound of Lefkada, NW Greece. Global and Planetary Change 66, 112-128.

Wick, L., Lemcke, G., Sturm, M., 2003. Evidence of Lateglacial and Holocene climatic change and human impact in eastern Anatolia: high-resolution pollen, charcoal, isotopic and geochemical records from the laminated sediments of Lake Van, Turkey. The Holocene 13, 665-675.

Wilson, A., 2013. The aqueduct of Butrint, In: Hansen, I.L., Hodges, R., Leppard, S. (Eds.), Butrint 4. The archaeology and histories of an Ionian Town. Oxbow Books, Oxford (United Kingdom), pp. 77-96.

Willis, K.J., 1992. The late Quaternary vegetational history of northwest Greece. New Phytologist 121, 101-117.

Wirth, S.B., Glur, L., Gilli, A., Anselmetti, F.S., 2013. Holocene flood frequency across the Central Alps – solar forcing and evidence for variations in North Atlantic atmospheric circulation. Quaternary Science Reviews 80, 112-128.

Woodbridge, J., Roberts, N., 2011. Late Holocene climate of the Eastern Mediterranean inferred from diatom analysis of annually-laminated lake sediments. Quaternary Science Reviews 30, 3381-3392.

Zanchetta, G., Van Welden, A., Baneschi, I., Drysdale, R., Sadori, L., Roberts, N., Giardini, M., Beck, C., Pascucci, V., Sulpizio, R., 2012. Multiproxy record for the last 4500 years from Lake Shkodra (Albania/Montenegro). Journal of Quaternary Science 27, 780-789.

Zhang, X., Reed, J., Wagner, B., Francke, A., Levkov, Z., 2014. Lateglacial and Holocene climate and environmental change in the northeastern Mediterranean region: diatom evidence from Lake Dojran (Republic of Macedonia/Greece). Quaternary Science Reviews 103, 51-66.

TABLE CAPTIONS

Comp depth (cm)	*Unit*	*Laboratory code*	*Type of material*	*AMS ^{14}C age (yr B.P.)*	*Calibrated age (cal yrs BP) (2σ range)*
348,6	A	ETH-48488	charcoal	1012 ± 26	889 ± 85
537,2	A	ETH-48489	charcoal	2233 ± 99	2314 ± 363
614,2	A	ETH-48490	charcoal	2468 ± 27	2548 ± 168
694,9	A	ETH-48491	charcoal	2791 ± 28	2878 ± 82
755,4	A	ETH-48492	charcoal	3155 ± 33	3356 ± 96
945,1	B	ETH-48493	wood	3232 ± 28	3470 ± 87
1021,1	C	ETH-48494	charcoal	3512 ± 33	3786 ± 91

Table 1. Radiocarbon dates used for the construction of the age model for the Lake Butrint sequence. Dates were calibrated using Calib 6.0 software and the INTCAL13 curve (Reimer et al., 2013); and the mid-point of 95.4% (2σ probability interval) was selected.

Settlement phases	*Human activities and historical events*	*Settlement intensity*
Mid- Late Bronze Age (Before 800 BC)	- Incipient grazing, shepherding and deforestation around Konispol Cave (Schuldenrein, 2001) - Small hilltop refuge intermittently occupied in Butrint Peninsula	1
Archaic (800 – 600 BC)	- Reoccupation of an unfortified, seasonal refuge with a sanctuary	1
Classical (600 – 300 BC)	- Earliest fortifications - Expansion of the settlement to 8 Ha within the Acropolis Hill - Harbor in the northern side of the peninsula	2
Hellenistic (300 – 100 BC)	- 3rd century BC: Expansion of the city wall to the south - 2nd century BC: incorporation of the northern citadel	3
Republican and early Imperial (100 BC – 100 AD)	- 31 – 0 BC: Foundation of the Roman city. Duplication of Hellenistic city surface and expansion towards the Vivari Channel shore - Late 1st century AD: Construction of the aqueduct-bridge and expansion of the city to the Vrina Plain, with the development of a suburb and associated centuriated landscape - Blocking of the Vivari Channel for marine vessels. Harbor located seawards from the aqueduct	4
Mid-Roman (100 – 300 AD)	- Increase in water supply to the city, with not significant urbanistic changes - Expansion of the Vrina Plain settlement	4
Late antique (300 – 700 AD)	- 4th century BC: Seismic event damaging parts of the city - Late 4th – early 5th centuries AD: Breakdown of the aqueduct - Economic revival from ~400 to 550 AD - Early-Mid 6th century AD: maximum dated findings of cattle remains (Powell, 2004) - 6th century AD: addition of a circuit wall along the shore of the Vivari Channel and Butrint Peninsula isthmus. Construction of the Great Basilica - 7th century AD: decline of the city	5
Early medieval (700 – 900 AD)	- ca. 800 AD: Attack and sack of Butrint by the Slavs - Drastic decrease/abandonment of the city, probably contracted to a small *castrum* in the acropolis - Gap in archaeological and documentary sources	1
High medieval (900 – 1300 AD)	- End of the 9th century AD: reappearance of Butrint in both archaeological and documentary sources - 9th-10th centuries AD: small initial settlement - After late 11th-13th centuries expansion of the urban centre to most of fortified areas. Evidences of landscaping and	3

	tenemental divisions. Intensification of farming in Vrina Plain. - ca. 13th century AD: reconstruction of wall circuits in the city. Dessertion of Vrina Plain Church and community for increasing waterlogging. Onset of swamp conditions.	
Late medieval / Venetian (1300 – 1797 AD)	- 1386 AD: Venetian occupation - Addition of towers to the Vivari Channel circuit - 15th century AD: Construction of the Triangular Fortress - Shift of constructions towards the mouths of Vivari Channel and Pavllo River - Frequent Ottoman attacks - Terminal economic decline. Abandonment of most of the old city in 1572 AD after Battle of Lepanto	2
Ottoman (1797 – 1912 AD)	- 1797 AD: Ottoman conquest - Abandonment or sporadic light occupation of the city	1
Independent Albania (After 1912 AD)	- 1928-1940 AD: Italian archaeological mission - 1960s – 1970s AD: Drainage and intensification of farming in the Vrina Plain - 1992 AD: Butrint listed on the UNESCO World Heritage	5

Table 2. Settlement phases in the ancient city of Butrint and surrounding areas with a summary of the main human activities and historical events (modified from Martin, (2004) and (Hodges, 2013) and an estimation of settlement intensity for each stage (1-5) based on available archaeological information: 0, sporadic-very low; 1, permanent-low; 2, permanent-low to moderate; 3, permanent-moderate; 4, high; and 5, very high).

FIGURE CAPTIONS.

Figure 1. (A) Satellite image of the study area within the Central Mediterranean region; (B) Close-up of Lake Butrint and adjacent areas; (C) bathymetric map with the location of the coring site BUT-12 (black dot) with the surveyed seismic grid (blue lines) and indication of the seismic profile displayed below (red line) (modified from Ariztegui et al. (2010); and (D) W-E seismic profile with two arrows indicating steep lake basin slopes likely related to normal faulting.

Figure 2. High resolution core images of the different sedimentary facies defined for the Lake Butrint sequence. (A-D) laminated, including: facies 1 with different proportions and thicknesses of yellow-calcitic, brown-organic and light-grey-clastic laminae (A-C) and barely laminated facies 2 (D). (E-H) massive facies, comprising: facies 3 (E), variegated facies 4 (F-G), both intercalated within laminated facies 1; and 5 (H). Scale is in cm.

Figure 3. Physical properties for the composite sequence of the Lake Butrint record. From left to right: core image, sedimentary units and subunits, sedimentological profile (see lithological legend below), magnetic susceptibility (MS) (SI units) at full scale (thick red line) and at reduced scale (2 to 28 10^{-5} SI, thin orange line), density (g/cc), colour parameters L* (greyscale), a* (green-red), b* (blue-yellow) and chronological scale (in cal years AD/BC). Homogenites are indicated with grey shaded horizontal bars.

Figure 4. Compositional parameters for the composite sequence of the Lake Butrint record. From left to right: core image, sedimentary units and subunits, sedimentological profile (see lithological legend in Fig. 2), Total Inorganic Carbon (TIC), Total Organic Carbon (TOC), Total Nitrogen (TN), Atomic TOC/TN ratio, Biogenic Silica (Bi Si),

mineralogical composition, including: quartz (Qtz), potassium feldspar (FdK), phyllosilicates (Phy), calcite (Cc), high-magnesium calcite (HMC), gypsum (Gy), Halite (Ha) and Pyrite (Py) (see legend below); reconstructed depositional environments and chronological scale (in cal years AD/BC).

Figure 5. X-ray Fluorescence (XRF) core scanner data for the Lake Butrint record. Element concentrations (K, Si, Ti, Fe, Mn, S, Ca and Sr) are expressed as counts per second, and Si/Ti, Fe/Mn and Ti/Ca ratios are indicated. Core image, sedimentary units and subunits sedimentological profile and chronological scale (in cal years AD/BC) are also included (see legend in Fig. 2).

Figure 6. Selected Non Pollen Palynomorphs (NPPs) and pollen curves for the Lake Butrint sequence. AP: arboreal pollen, NAP: non-arboreal pollen. Arrows in the lower part of the figure indicate the interpretation of each taxon. Core image, sedimentary units and subunits sedimentological profile and chronological scale (in cal years AD/BC) are also included (see legend in Fig. 2).

Figure 7. (A) AMS calibrated radiocarbon dates (black dots with error bars) and ^{137}Cs maximum peaks of 1986 AD and 1963 AD (red dots), represented in an age vs depth plot for the Lake Butrint sequence, with homogenites represented by horizontal grey bars. (B) Chronological model for the event-corrected (i.e., without homogenites) depth scale of the sequence, based on the linear interpolation of calibrated radiocarbon dates and maximum ^{137}Cs peaks. Sedimentary units and subunits are represented at the left side of the figure.

Figure 8. Selected plots of proxy data analyzed in the Lake Butrint sequence (lower part) with other regional and global records (upper part) for the last ~4 cal kyrs BP. In the lower section, from bottom to top: settlement phases and estimated intensities (1-5)

for the ancient city of Butrint, paleoenvironmental reconstruction for the different units (A-B-C) and subunits, calibrated radiocarbon dates, homogeneous layers (H-layers) thickness, Chenopodiaceae and *Alnus* pollen concentrations (%), Ti/Ca ratio, Ca (cps), Sr (cps) and Fe/Mn ratio. A grey shaded vertical bar indicates the maximum occupation period in Butrint city. In the upper section: lakes Ohrid (Lacey et al., 2014) and Prespa (Leng et al., 2013) $\delta^{18}O$ records, Lake Dojran potassium (K) record (in cps) (Zhang et al., 2014), Lake Nar (Dean et al., 2015; Jones et al., 2006) and Soreq Cave (Bar-Matthews et al., 2003) $\delta^{18}O$ records. Note that records are aligned across a West (lower) to East (upper) gradient. At the uppermost part of the record, reconstruction of NAO index carried out by Olsen et al. (2012) and Global Temperature (T) reconstructed anomalies (Marcott et al., 2013) and main Late Holocene climatic stages (Little Ice Age (LIA), Medieval Climate Anomaly (MCA), Early Middle Ages (EMA), Roman Warm Period (RWP) and Subatlantic/Sub-boreal periods). Vertical dotted lines represent temporal subdivisions used in the Discussion section.

1396

Table 1

Comp depth (cm)	*Unit*	*Laboratory code*	*Type of material*	*AMS ^{14}C age (yr B.P.)*	*Calibrated age (cal yrs BP) (2σ range)*
348,6	A	ETH-48488	charcoal	1012 ± 26	889 ± 85
537,2	A	ETH-48489	charcoal	2233 ± 99	2314 ± 363
614,2	A	ETH-48490	charcoal	2468 ± 27	2548 ± 168
694,9	A	ETH-48491	charcoal	2791 ± 28	2878 ± 82
755,4	A	ETH-48492	charcoal	3155 ± 33	3356 ± 96
945,1	B	ETH-48493	wood	3232 ± 28	3470 ± 87
1021,1	C	ETH-48494	charcoal	3512 ± 33	3786 ± 91

Table 1. Radiocarbon dates used for the construction of the age model for the Lake Butrint sequence. Dates were calibrated using Calib 6.0 software and the INTCAL13 curve (Reimer et al., 2013); and the mid-point of 95.4% (2σ probability interval) was selected.

Table 2

Settlement phases	*Human activities and historical events*	*Settlement intensity*
Mid- Late Bronze Age (Before 800 BC)	- Incipient grazing, shepherding and deforestation around Konispol Cave (Schuldenrein, 2001) - Small hilltop refuge intermittently occupied in Butrint Peninsula	1
Archaic (800 – 600 BC)	- Reoccupation of an unfortified, seasonal refuge with a sanctuary	1
Classical (600 – 300 BC)	- Earliest fortifications - Expansion of the settlement to 8 Ha within the Acropolis Hill - Harbor in the northern side of the peninsula	2
Hellenistic (300 – 100 BC)	- 3rd century BC: Expansion of the city wall to the south - 2nd century BC: incorporation of the northern citadel	3
Republican and early Imperial (100 BC – 100 AD)	- 31 – 0 BC: Foundation of the Roman city. Duplication of Hellenistic city surface and expansion towards the Vivari Channel shore - Late 1st century AD: Construction of the aqueduct-bridge and expansion of the city to the Vrina Plain, with the development of a suburb and associated centuriated landscape - Blocking of the Vivari Channel for marine vessels. Harbor located seawards from the aqueduct	4
Mid-Roman (100 – 300 AD)	- Increase in water supply to the city, with not significant urbanistic changes - Expansion of the Vrina Plain settlement	4
Late antique (300 – 700 AD)	- 4th century BC: Seismic event damaging parts of the city - Late 4th – early 5th centuries AD: Breakdown of the aqueduct - Economic revival from ~400 to 550 AD - Early-Mid 6th century AD: maximum dated findings of cattle remains (Powell, 2004) - 6th century AD: addition of a circuit wall along the shore of the Vivari Channel and Butrint Peninsula isthmus. Construction of the Great Basilica - 7th century AD: decline of the city	5
Early medieval (700 – 900 AD)	- ca. 800 AD: Attack and sack of Butrint by the Slavs - Drastic decrease/abandonment of the city, probably contracted to a small *castrum* in the acropolis - Gap in archaeological and documentary sources	1
High medieval (900 – 1300 AD)	- End of the 9th century AD: reappearance of Butrint in both archaeological and documentary sources - 9th-10th centuries AD: small initial settlement - After late 11th-13th centuries expansion of the urban centre to most of fortified areas. Evidences of landscaping and	3

	tenemental divisions. Intensification of farming in Vrina Plain. - ca. 13th century AD: reconstruction of wall circuits in the city. Dessertion of Vrina Plain Church and community for increasing waterlogging. Onset of swamp conditions.	
Late medieval / Venetian (1300 – 1797 AD)	- 1386 AD: Venetian occupation - Addition of towers to the Vivari Channel circuit - 15th century AD: Construction of the Triangular Fortress - Shift of constructions towards the mouths of Vivari Channel and Pavllo River - Frequent Ottoman attacks - Terminal economic decline. Abandonment of most of the old city in 1572 AD after Battle of Lepanto	2
Ottoman (1797 – 1912 AD)	- 1797 AD: Ottoman conquest - Abandonment or sporadic light occupation of the city	1
Independent Albania (After 1912 AD)	- 1928-1940 AD: Italian archaeological mission - 1960s – 1970s AD: Drainage and intensification of farming in the Vrina Plain - 1992 AD: Butrint listed on the UNESCO World Heritage	5

Table 2. Settlement phases in the ancient city of Butrint and surrounding areas with a summary of the main human activities and historical events (modified from Martin, (2004) and (Hodges, 2013) and an estimation of settlement intensity for each stage (1-5) based on available archaeological information: 0, sporadic-very low; 1, permanent-low; 2, permanent-low to moderate; 3, permanent-moderate; 4, high; and 5, very high).

Figure 1

Click here to download high resolution image

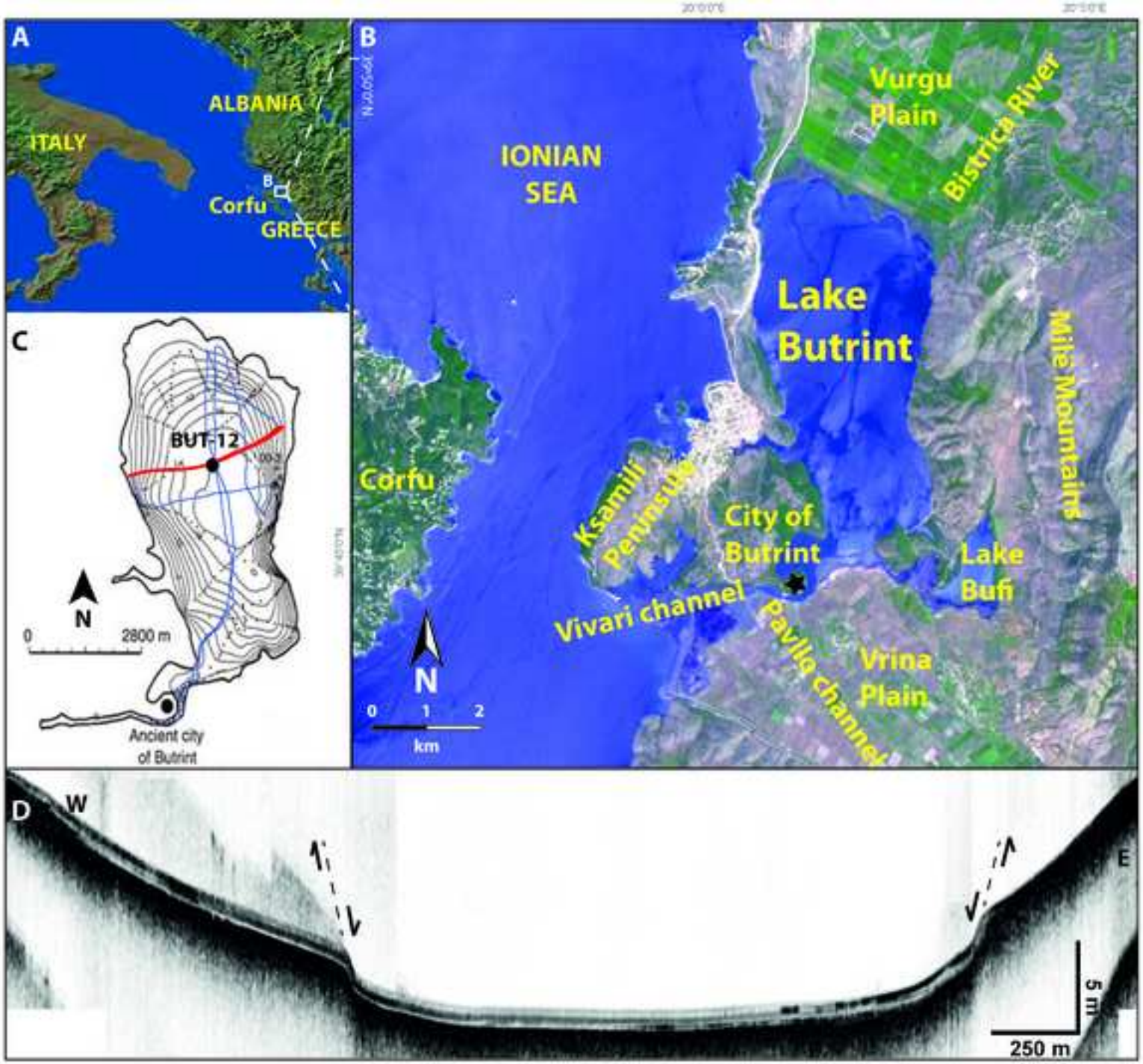

Figure 2

Click here to download high resolution image

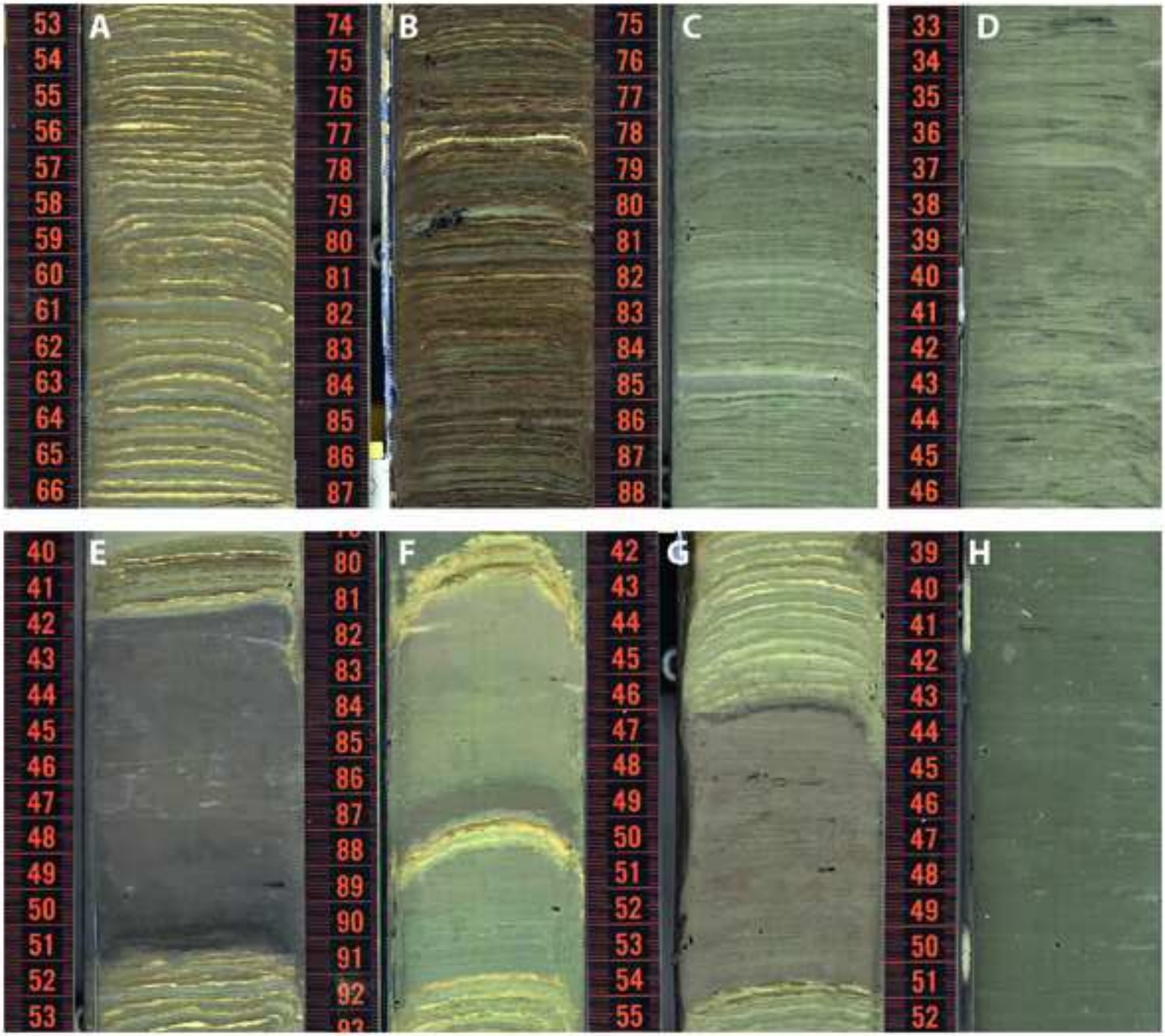

Figure 3

Click here to download high resolution image

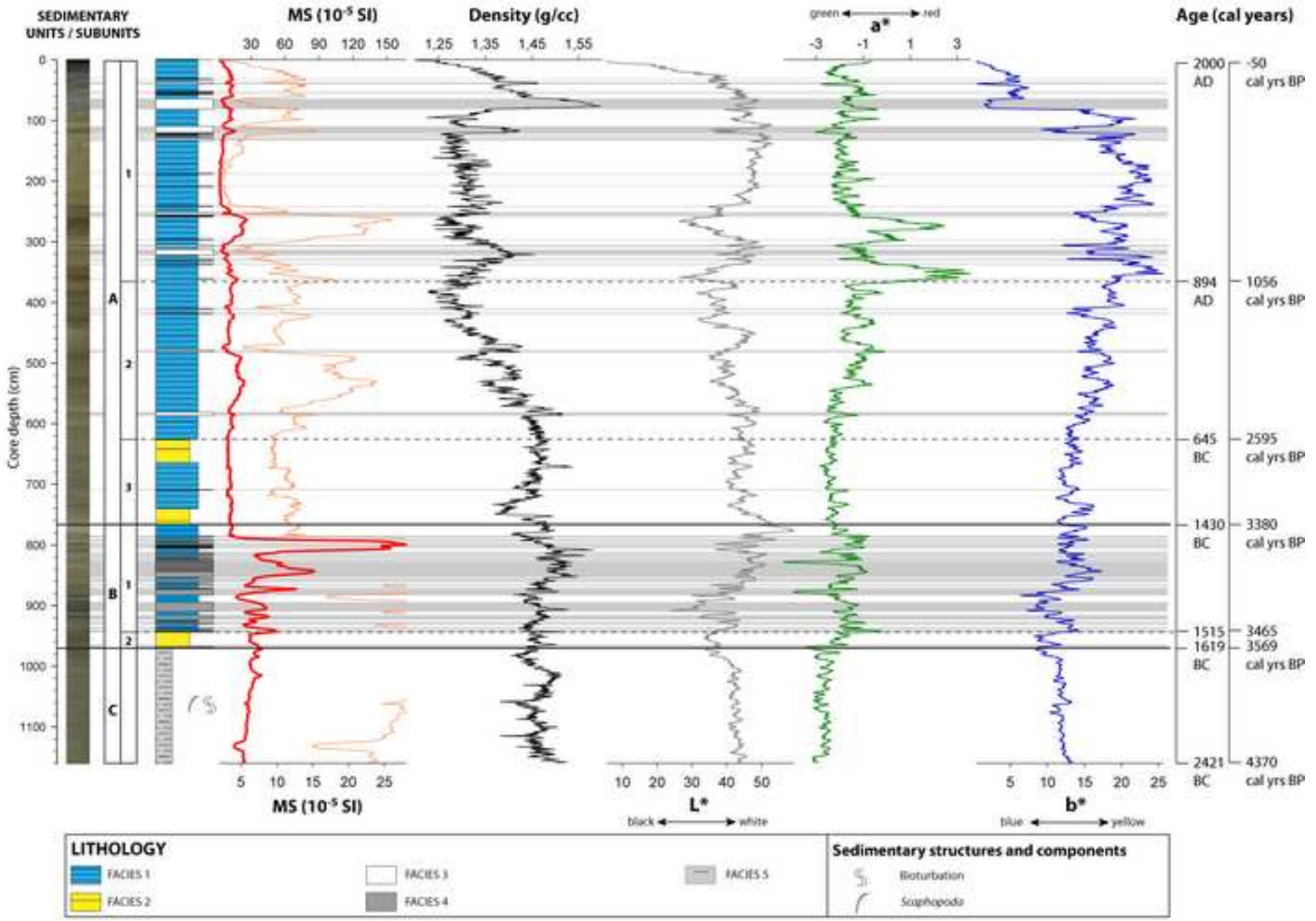

Figure 4

Click here to download high resolution image

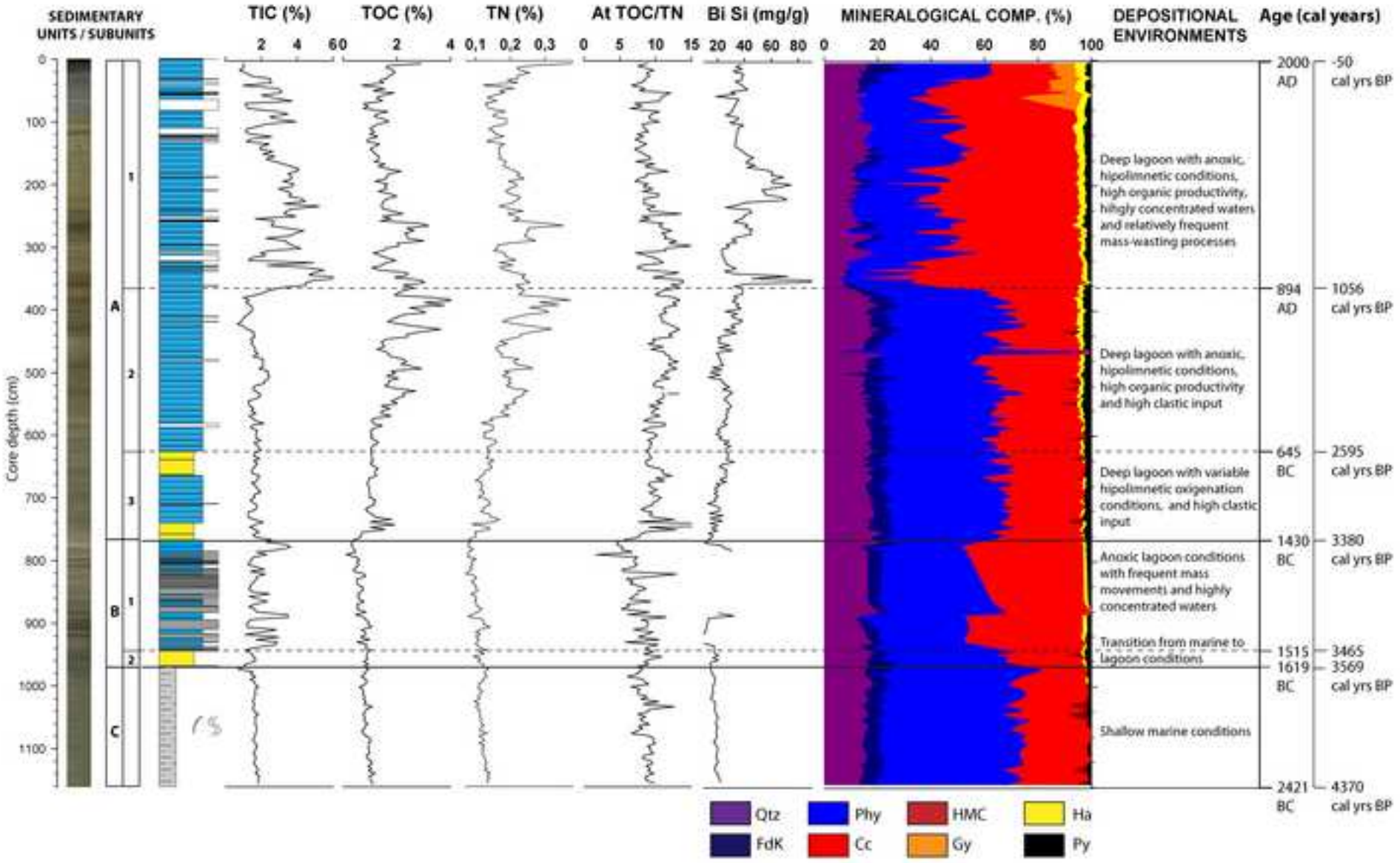

Figure 5

Click here to download high resolution image

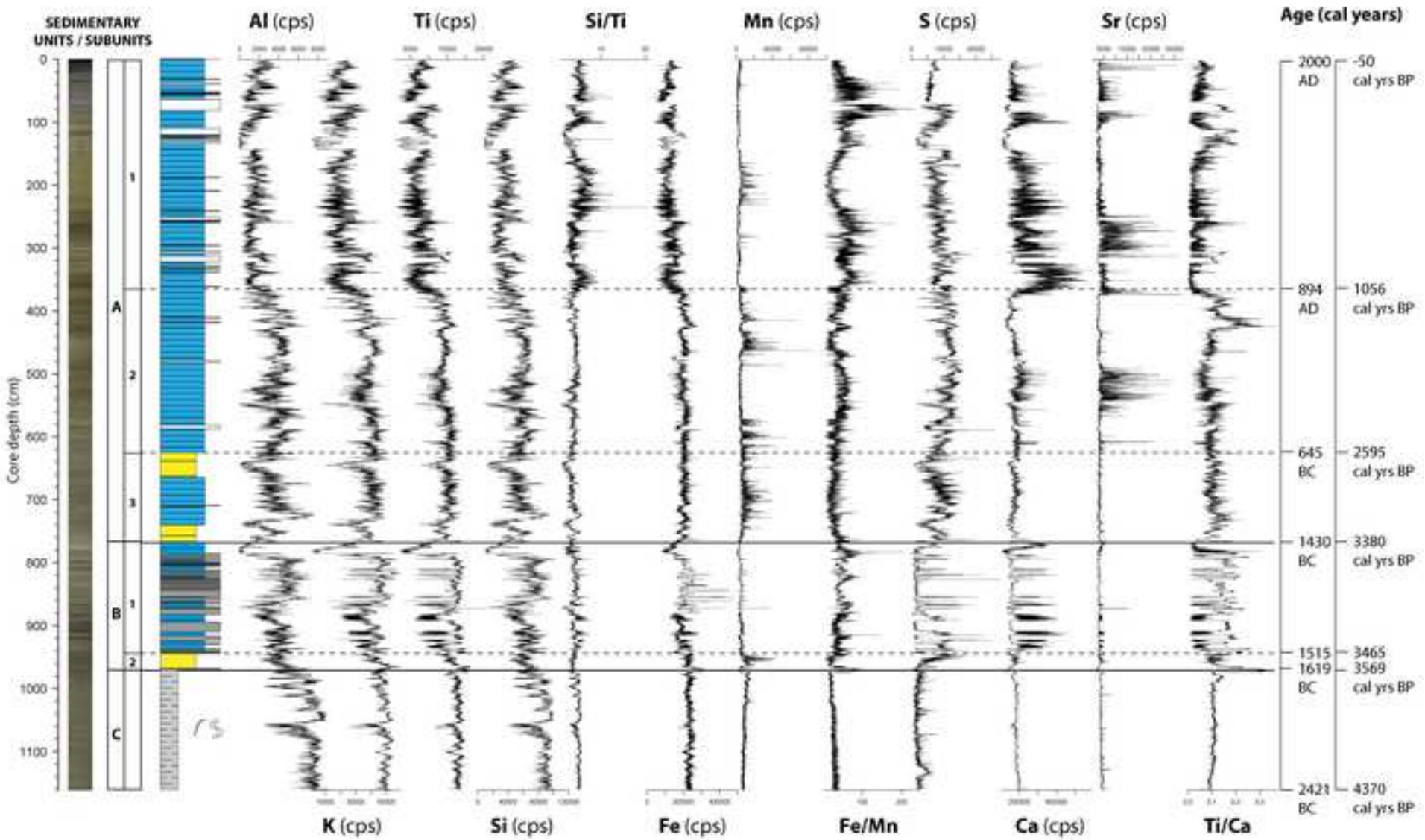

Figure 6

Click here to download high resolution image

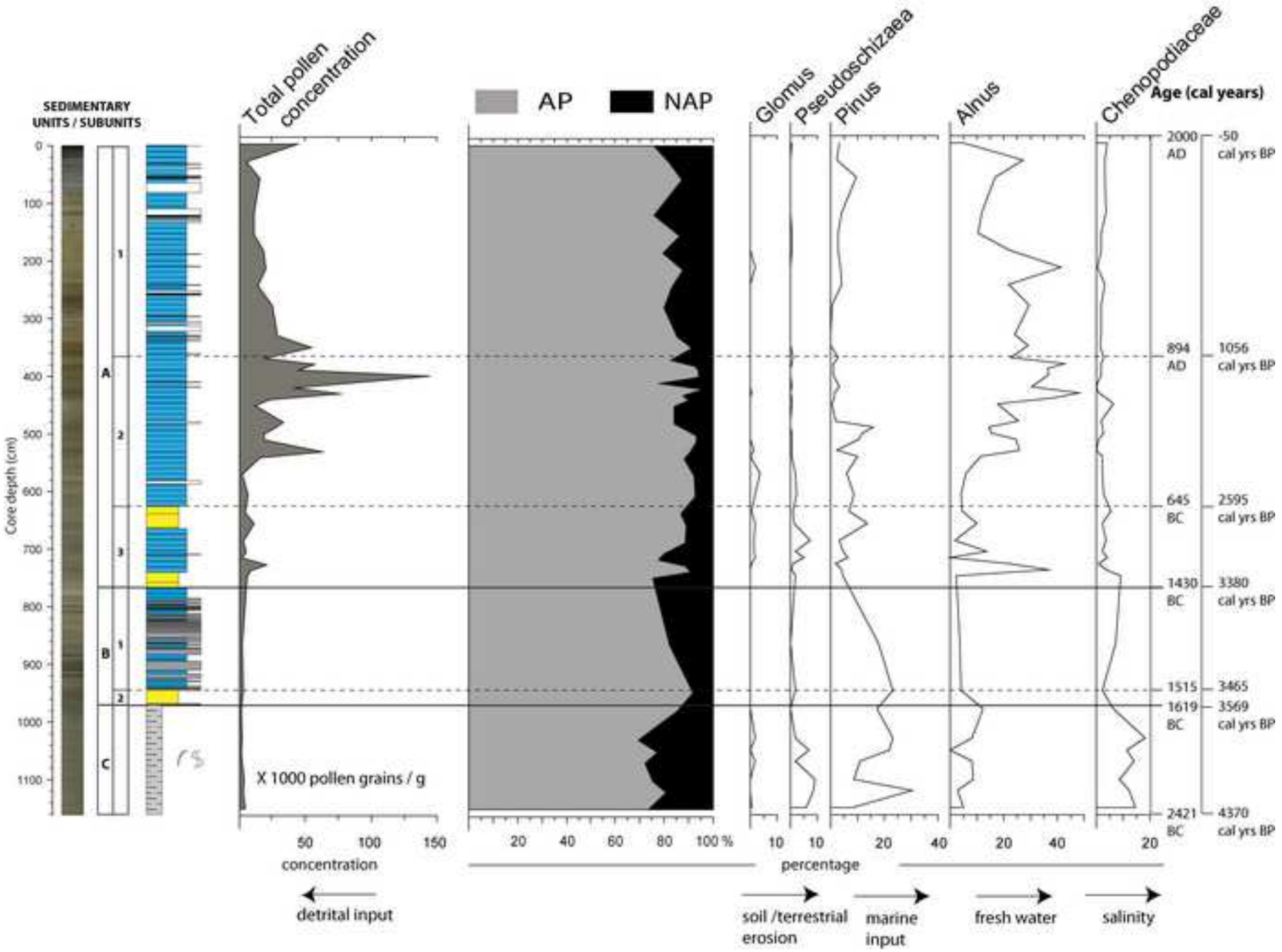

Figure 7

Click here to download high resolution image

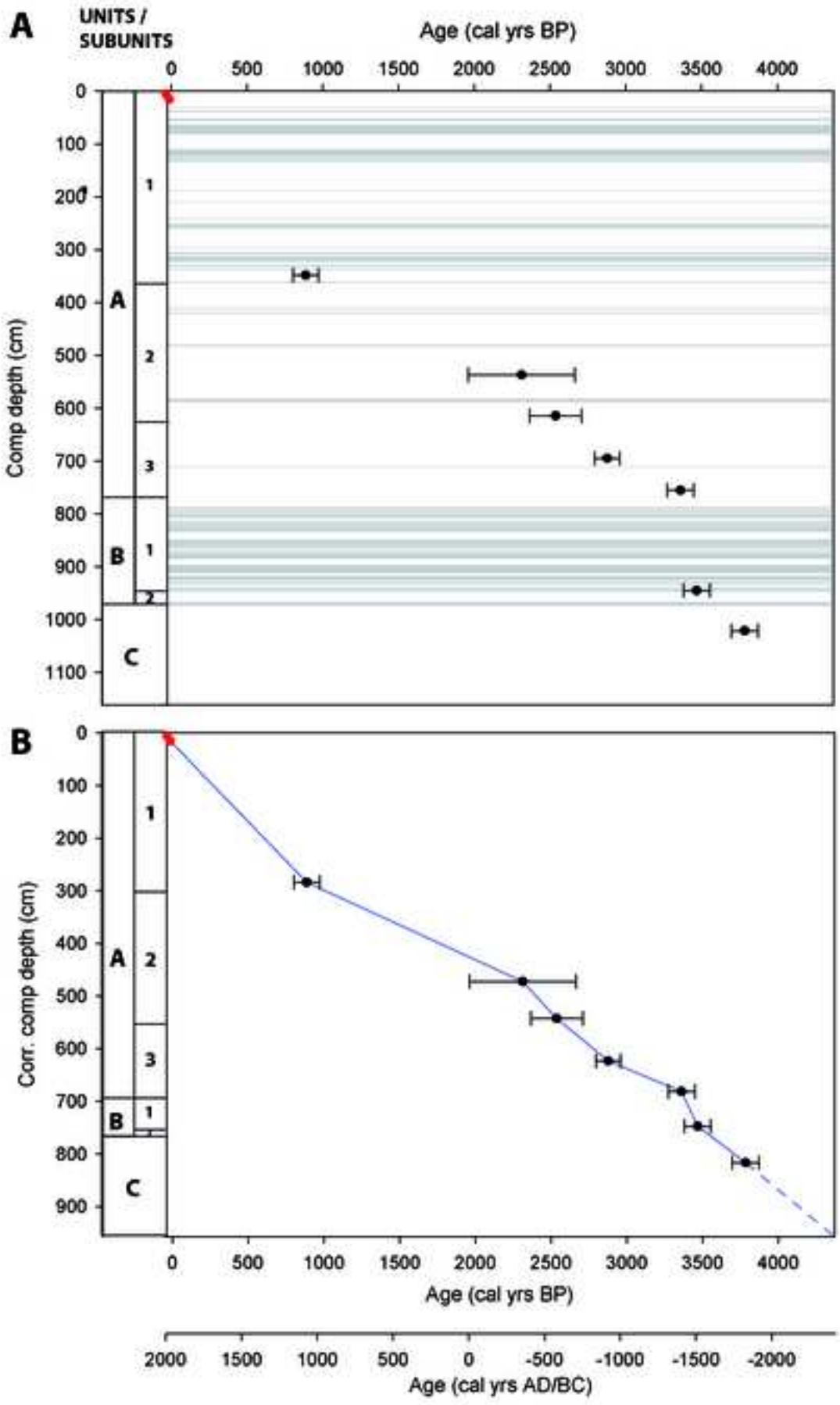

Figure 8

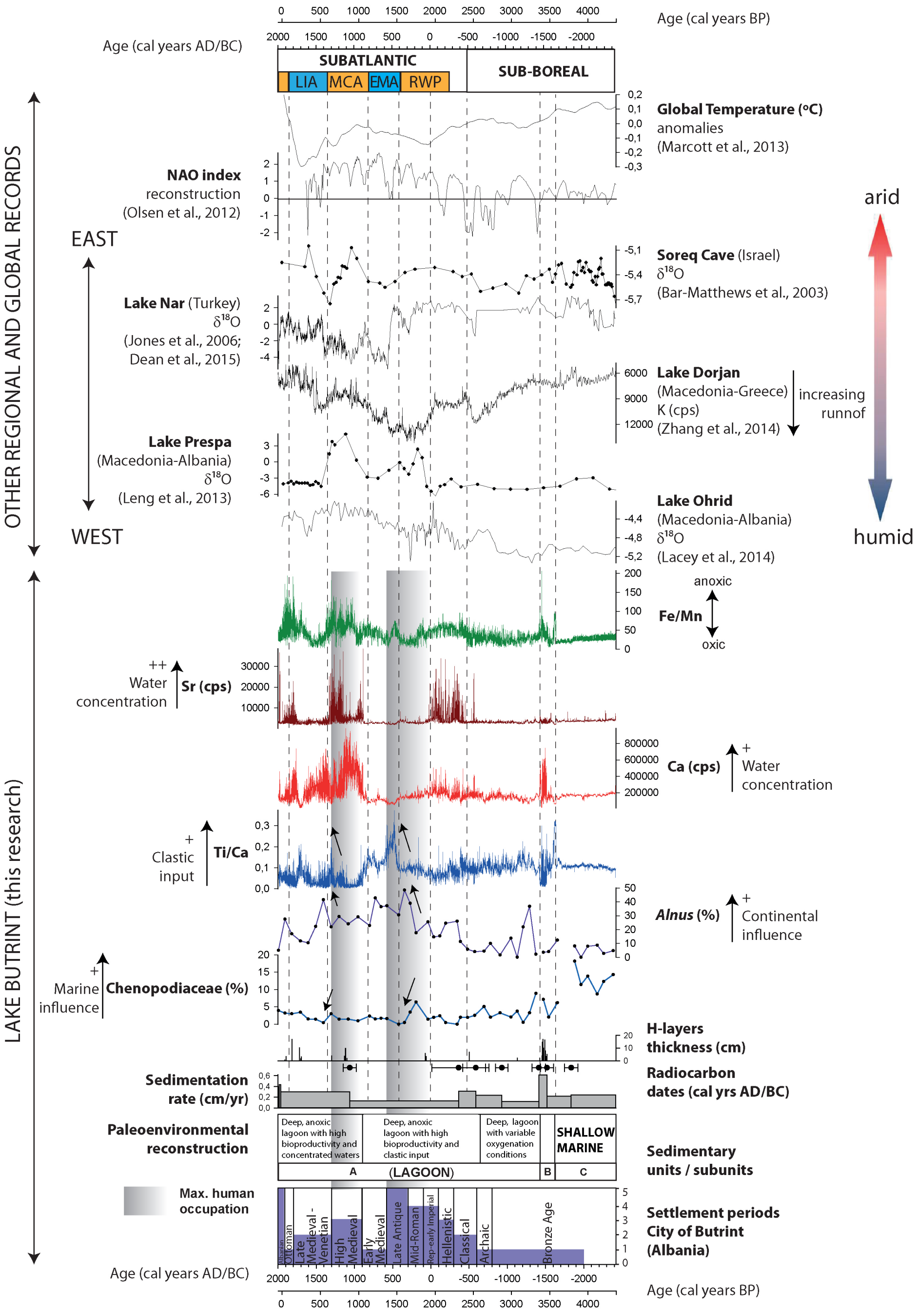
Age (cal years AD/BC)
Age (cal years BP)
SUBATLANTIC
SUB-BOREAL
LIA
MCA
EMA
RWP
Global Temperature (°C)
anomalies
(Marcott et al., 2013)
NAO index
reconstruction
(Olsen et al., 2012)
EAST
WEST
Lake Nar (Turkey)
δ18O
(Jones et al., 2006;
Dean et al., 2015)
Soreq Cave (Israel)
δ18O
(Bar-Matthews et al., 2003)
Lake Prespa
(Macedonia-Albania)
δ18O
(Leng et al., 2013)
Lake Dorjan
(Macedonia-Greece)
K (cps)
(Zhang et al., 2014)
increasing runnof
Lake Ohrid
(Macedonia-Albania)
δ18O
(Lacey et al., 2014)
arid
humid
anoxic
Fe/Mn
oxic
OTHER REGIONAL AND GLOBAL RECORDS
LAKE BUTRINT (this research)
++ Water concentration
Sr (cps)
Ca (cps)
+ Water concentration
+ Clastic input
Ti/Ca
Alnus (%)
+ Continental influence
+ Marine influence
Chenopodiaceae (%)
H-layers thickness (cm)
Radiocarbon dates (cal yrs AD/BC)
Sedimentation rate (cm/yr)
Paleoenvironmental reconstruction
Deep, anoxic lagoon with high bioproductivity and concentrated waters
Deep, anoxic lagoon with high bioproductivity and clastic input
Deep, lagoon with variable oxygenation conditions
SHALLOW MARINE
A
(LAGOON)
B
C
Sedimentary units / subunits
Max. human occupation
Albanian
Ottoman
Late Medieval - Venetian
High Medieval
Early Medieval
Late Antique
Mid-Roman
Rep-early Imperial
Hellenistic
Classical
Archaic
Bronze Age
Settlement periods City of Butrint (Albania)
Age (cal years AD/BC)
Age (cal years BP)

HIGHLIGHTS

- Reconstruction of Late Holocene environmental changes in the Central Mediterranean
- Tectonics, climate and human activities controlled Lake Butrint recent evolution
- Maximum human settlement intensity coincides with moister and more stable climate
- Short-term hydrological changes controlled by NAO-driven climate variability
- Opposite hydrological patterns with Levantine records during the last 1000 years

Supplementary Data

Click here to download Supplementary Data: Supplementary Data.xlsx